

Review

Research and Development Review of Power Converter Topologies and Control Technology for Electric Vehicle Fast-Charging Systems

Kai Zhou ¹, Yanze Wu ¹, Xiaogang Wu ^{1,2,*}, Yue Sun ¹, Da Teng ¹ and Yang Liu ¹

¹ Engineering Research Center of Automotive Electronics Drive Control and System Integration (Ministry of Education), Harbin University of Science and Technology, Harbin 150080, China

² State Key Laboratory of Automotive Safety and Energy, Tsinghua University, Beijing 100084, China

* Correspondence: xgwu@hrbust.edu.cn; Tel.: +86-136-3360-1003

Abstract: With the rapid development of the electric vehicle (EV) industry, charging facilities for electric vehicles are gradually improving, thus meeting the demand for fast and safe charging. This paper comprehensively describes the current development status and future development trend of EVs and their charging infrastructure and analyzes in detail the EV fast-charging system architecture according to the AC/DC coupling configuration. The topologies and control techniques of the front AC/DC converter and rear DC/DC converter for the charging system are discussed, providing a reference for the future design of hundred-kilowatt level and above fast-charging systems for EVs. In addition, this paper summarizes the EV charging interface and the charging specifications applicable to the hundred-kilowatt power fast-charging system, as well as the impact of fast charging on power batteries, and emphasizes that high-power fast-charging technology is an inevitable trend for the future development of electric vehicles.

Keywords: electric vehicle; fast-charging system; AC/DC converter; DC/DC converter; charging control technology



Citation: Zhou, K.; Wu, Y.; Wu, X.; Sun, Y.; Teng, D.; Liu, Y. Research and Development Review of Power Converter Topologies and Control Technology for Electric Vehicle Fast-Charging Systems. *Electronics* **2023**, *12*, 1581. <https://doi.org/10.3390/electronics12071581>

Academic Editor: Lazhar Ben-Brahim

Received: 15 February 2023

Revised: 10 March 2023

Accepted: 14 March 2023

Published: 28 March 2023



Copyright: © 2023 by the authors. Licensee MDPI, Basel, Switzerland. This article is an open access article distributed under the terms and conditions of the Creative Commons Attribution (CC BY) license (<https://creativecommons.org/licenses/by/4.0/>).

1. Introduction

In recent years, people's awareness of resource conservation and environmental protection has gradually increased. EVs have progressively become the main development direction of the automotive industry due to their low pollution and low cost of use. They are also driving the development of other sectors in their industrial chain [1]. Compared to traditional fuel vehicles, EVs have three obvious advantages: their energy has two-way mobility, the electronic technology supporting them is mature and specialized, and they have low carbon emissions [2].

In this context, governments and automotive companies are gradually reducing the production of conventional fuel vehicles and shifting their R&D focus to EVs. As a result, annual EV sales have rapidly increased. In 2021, global sales of EVs reached 6.6 million units, which was double the number sold in 2020. In 2012, only 120,000 EVs were sold worldwide, whereas more than that number were sold on a weekly basis in 2021 [3]. Figure 1 shows the global EV inventory from 2010 to 2021. In 2021, the total global EV inventory was over 16.5 million, which was three times the number in 2018. By 2030, global EV stock is expected to exceed 150 million [4].

The industrialization of EVs is a system project and the charging infrastructure is one of the most important links. The charging system is an integral part of the charging infrastructure and provides energy replenishment for the operation of EVs in addition to being an important support system for EVs [5]. Charging systems need to be compatible with the battery system of EVs and are classified into slow-charging systems and fast-charging systems based on their power. Slow-charging systems are typically capable of

outputting 3–4 kW of power and take about 8–10 h to fully charge a battery. They are mostly used for charging at night and utilize a home’s grid power. Fast-charging systems can output hundreds of kilowatts of power and the charging time is usually less than one hour. Additionally, they can be installed in public places or gas stations [6].

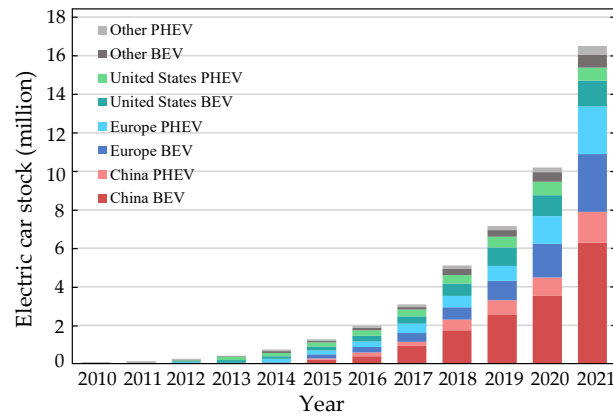


Figure 1. Global electric vehicle inventory (2010–2021).

Long-range capabilities and shorter charging times have become the main focus of technological innovation for EVs, and the availability and stability of the corresponding public charging facilities are crucial to their success [7]. Figure 2 shows the distribution of public EV charging systems by power level and region from 2015 to 2021. China has about 85% of the world’s fast-charging systems and 55% of the world’s slow-charging systems. In 2021, the number of fast-charging systems in China reached about 470,000 units, an increase of 44% from 2020. Similarly, the number of slow-charging systems in China in 2021 reached about 680,000 units, which was 35% more than in 2020 and more than four times the number in 2018. There are about 22,000 fast charging systems in the United States, nearly 60% of which are Tesla supercharging systems [8,9].

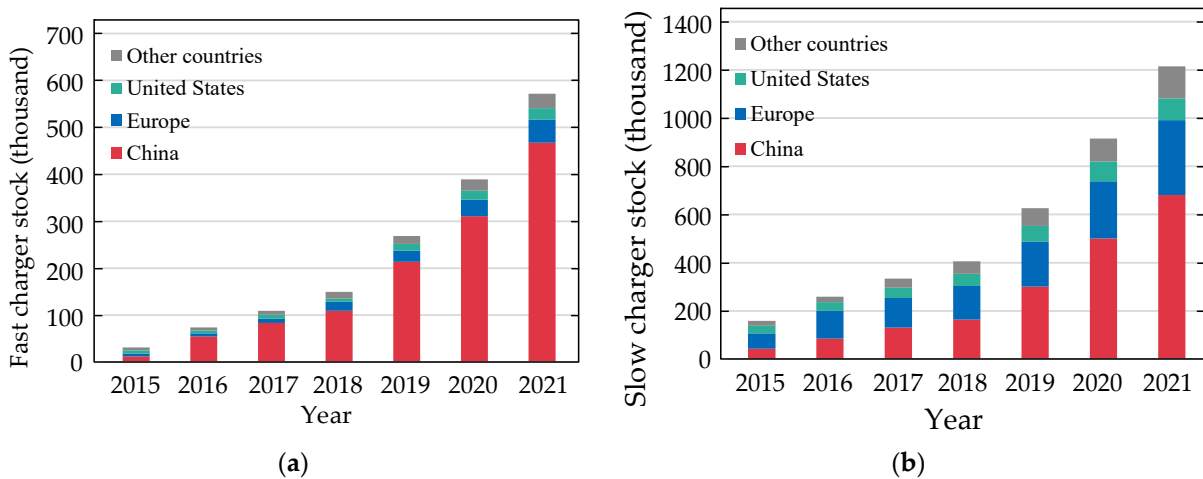


Figure 2. Public electric vehicle charging system by power level and region (2015–2021). (a) Publicly available fast chargers. (b) Publicly available slow chargers.

With the development of fast-charging technology, experiments have shown that the theoretical charging time of batteries can be shortened to as little as 3 min. A large number of 100 kW power charging systems connected to the grid at the same time can significantly impact the grid, including the power quality (harmonic current, voltage offset, voltage imbalance at the incoming nodes), grid economy (line and transformer losses), and operational stability (grid waveform, peak load, electrical facility life) [10–13]. Increasing

the load capacity of the distribution grid can fundamentally solve these problems but is costly. Numerous scholars in China and elsewhere have conducted extensive research on designing fast-charging systems that can meet the regional base grid's demands of 100 kW power. Their research includes circuit topology, operation control of charging systems, and the proposal of new topologies. They have also explored the incorporation of renewable energy systems and battery storage systems, as well as the use of Vehicle-to-Grid (V2G) technology and the corresponding control strategies to ensure that fast-charging systems can meet short-time high-power load demand [14,15]. The research mainly focuses on whether the circuit topology can meet the power level of the charging station, voltage and current entry standards, and other requirements. EV charging systems can be divided into on-board and off-board types, each with unidirectional and bidirectional power mobility. This paper will mainly discuss the circuit topology and related control methods suitable for the 100 kW power level.

Numerous references related to fast-charging technology have been compiled and studied. In [16,17], the current state of research regarding fast-charging schemes and electrical topologies was analyzed. In [17], the fast-charging station's overall architecture and control strategies were studied and analyzed at the University of Naples as an example of a charging unit. The AC/DC and DC/DC power converters for fast-charging systems were analyzed in detail in [18–21]. A resonant DC/DC converter with a modular parallel structure was proposed in [19], which can increase the power rating and reliability of the charging system. The fast-charging system can be divided into unidirectional and bidirectional charging systems according to the power flow direction. A bidirectional DC fast-charging system was proposed in [20], which uses a dual-active-bridge (DAB) converter with blocking capacitors and an active front-end converter and can realize bidirectional power flow between EVs and the grid. Traditional low-frequency transformers are widely used in power systems. However, because their use increases the weight and cost of charging systems and generates problems such as grid current harmonics, solid-state transformer (SST) technology has gradually begun to be applied in fast-charging systems. The architecture of SST-based ultra-fast-charging systems was introduced in [22–24]. The authors of [24] discussed current state-of-the-art fast-charging systems, the current status of the charging infrastructure, power converter topologies suitable for medium-voltage ultra-fast-charging stations, and the integration of renewable energy systems and energy storage systems. A fast-charging system consisting of a charging power converter system and a battery energy storage system was proposed in [25], which can meet the requirements for the fast-charging of high-power EVs. In order to reduce the impact of EV fast-charging stations on the grid, a two-stage centralized method was proposed in [26] to balance the power mismatch between the predicted and real-time demands of the medium-voltage grid and reduce grid losses. A two-stage model was proposed in [27] for solving the charging infrastructure design problem. The model considers the distribution grid capacity to maintain voltage stability and determine the optimal location and capacity with minimum deployment costs.

This paper first describes the current development of EVs and their charging infrastructure and summarizes the current literature on fast charging and ultra-fast charging. Section 2 analyzes EV fast-charging technology and the configuration of the EV charging system. Section 3 summarizes the charging interfaces and technical specifications for fast and ultra-fast charging. To realize the fast-charging requirements, the front AC/DC converter and rear DC/DC converter of fast-charging systems are described in Sections 4 and 5, respectively, and the corresponding control strategies are presented in Sections 6 and 7. Section 8 describes the impact of fast charging on the power battery and details various fast-charging methods. Section 9 introduces the future development trends of EV fast-charging technology and Section 10 presents the conclusions.

2. Electric Vehicle Fast-Charging Technology and System Structure

2.1. Charging Level of Electric Vehicles

EV charging systems can be divided into slow- and fast-charging systems. Slow-charging systems are generally defined as Level 1 and Level 2 on-board charging systems. Level 1 on-board charging systems are slow and take about 8–10 h to fully charge a power battery. They are primarily used in residential buildings and the output power is usually less than 10 kW. In contrast, Level 2 charging systems take less time than Level 1 systems to fully charge a battery. They are usually used in shopping malls, public facilities, etc., and the power can reach 20 kW [28].

Currently, there are two general topologies for slow-charging systems, namely on-board charging systems. One is a single-stage topology with an uncontrolled rectifier and high-frequency DC/DC converter. This topology includes forward, flyback, push-pull, half-bridge, and full-bridge. Single-stage topology has the advantages of a simple structure, smaller number of components, small size, etc., but because it is directly connected to the grid, it can easily pollute the grid. The other is a two-stage charging system with power factor correction in the front stage and a DC/DC converter in the rear stage. The two-stage charging system can effectively address the issues of the low power factor and serious harmonic pollution but it has a high cost and low efficiency. Currently, the conventional PID control method is widely used for slow-charging systems but more advanced control methods, such as BP neural network PID control methods and fuzzy adaptive PID control methods, have also been developed, which can significantly affect the charging output characteristics.

As the number of EVs in use has increased, so has consumer demand for faster charging systems, as slow-charging systems have a long charging time and low power output. Fast-charging systems are a type of non-vehicle charging system that can be classified into fast and ultra-fast types. The topology and control strategy of the off-board charging systems are described in detail in the following sections.

Fast-charging systems, also known as Level 3 charging systems, can deliver high currents of up to 400 A and can fully charge power batteries in 20–30 min, typically in the 50 kW–350 kW range. The ultra-fast-charging system is rated at 400 kW or even higher and can fully charge power batteries in 20 min. Due to the maturity of fast-charging technology, ultra-fast-charging systems have more application prospects. The interfaces and standards for fast- and ultra-fast-charging systems are presented in Section 3 of this paper. Table 1 shows the types and levels of EV charging, and Table 2 summarizes the current advanced fast/ultra-fast-charging systems with hundred-kilowatt power levels.

Table 1. Electric vehicle charging types and levels.

Charging Type	Charging Location	Specifications			Charging Time (Battery Capacity)	Criterion
		Voltage/V	Current/A	Power/kW		
Level 1	On-board	120/230	12–16	1.44–1.92	11–36 h (16–50 kWh)	International Electrotechnical Commission (IEC)
Level 2	On-board	208/240	15–80	3.1–19.2	2–6 h (16–30 kWh)	
Level 3 (Fast)	Off-board	300–600	≤400	50–350	≤30 min (20–50 kWh)	
Ultra-fast	Off-board	>800	>400	≥400	≈10 min (20–50 kWh)	

Table 2. Characteristics of the 100-kilowatt-class of fast/ultra-fast-charging systems.

Manufacturer and Model	Power/kW	Input Voltage/V	Output Voltage/V	Output Current/A	Supported Standards	Peak Efficiency/%	Weight/lbs
EVBox Troniq 100	100	480 Vac \pm 10%	500	200	CCS Combo 1, CHAdeMO	95	2535
PHIHONG Integrated Type	120	380/480 Vac \pm 10%	200–750	240	GB/T 20234.3	93.5	528
Tesla Supercharger	135	380–480 Vac	50–410	330	Super charger	91	1323
EVTEC espresso and charger	150	400 Vac \pm 10%	170–940	50–400	SAE Combo 1, CHAdeMO	93	881
Delta	200	400 Vac \pm 10%	200–1000	350–500	CHAdeMO, CCS	94	992
ABB Terra HP	350	400 Vac \pm 10%	150–920	500	SAE Combo 1, CHAdeMO 1.2	95	2954
Tritium Veefil PK	475	480 Vac	920	500	CHAdeMO, CCS	98.5	1540

2.2. Electric Vehicle Fast-Charging System Architecture

EV charging systems generally have a centralized layout in a specific area, and the power supply typically employs AC coupling or DC coupling, that is, multiple independent charging systems use the common AC bus or common DC bus to obtain power. The configuration is shown in Figure 3.

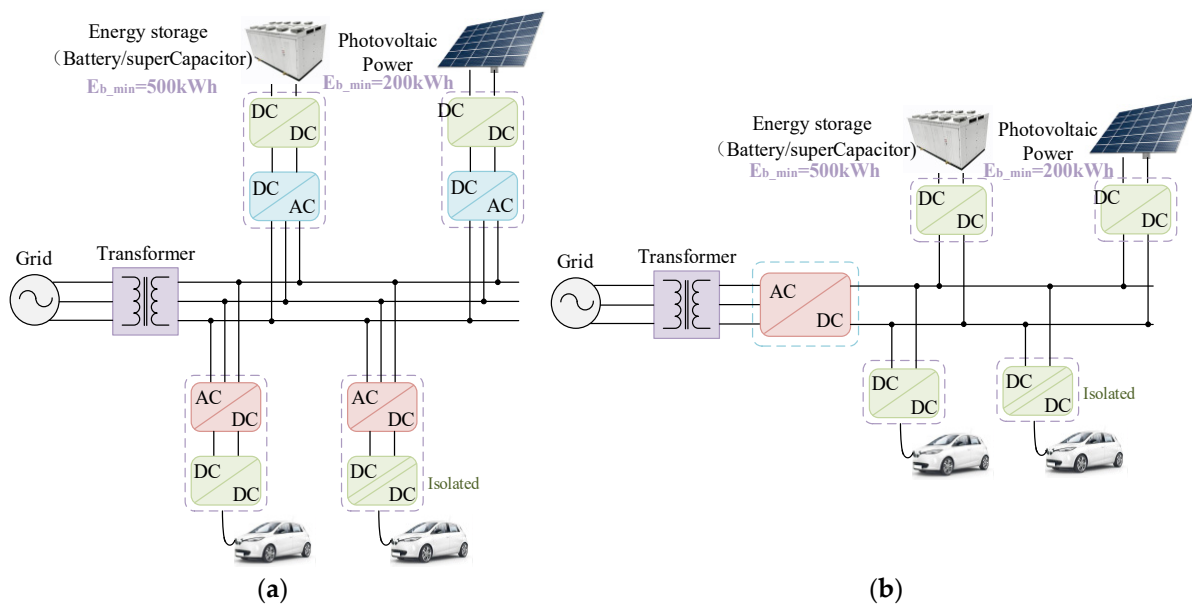


Figure 3. Electric vehicle fast-charging system architecture. (a) AC coupling configuration method. (b) DC coupling configuration method.

In the AC-coupled configuration, a low-frequency transformer is used to connect the medium-voltage grid to the common coupling point of the charging system to supply power to each independent charging system. Each charging system consists of an AC/DC converter and a DC/DC converter. Many charging systems use the AC coupling configuration because the converter technology is mature and the AC distribution system is stable. However, the overall complexity of system control is high since the power flow between the grid and the EV must pass through the AC bus and multiple AC/DC and DC/DC converters [29].

In the DC-coupled configuration, high-power AC/DC converters are connected to a low-frequency transformer, which is then coupled to the EV charging system through a DC

bus. This configuration uses centralized rectification, which effectively reduces the number of AC/DC converters, simplifies system control, and alleviates the impact of high-power charging on the grid [30]. The DC bus power supply structure is used to effectively avoid the problems of the power angle, frequency stability, and reactive loop current in the AC bus. The power flow between the grid and the EV can be controlled by detecting the magnitudes of the AC and DC side voltages and currents on the grid side. However, the DC/DC converters connected to EVs typically have an isolation-type structure, which means that each charging system needs to be equipped with high-frequency transformers. However, the primary and secondary circuits of these high-frequency transformers still need to be controlled independently, which results in a high level of complexity in the control system of the charging station's rear stage [31,32].

The fast-charging system consists of two AC/DC conversion stages: the first is the rectification stage that converts three-phase AC power to high-voltage DC power, i.e., AC/DC, which includes power factor correction (PFC) to improve power utilization effectively. The second stage is the conversion of high-voltage DC power to DC power that matches the voltage level of the load, i.e., DC/DC. Typically, an EV charging strategy involves the battery constant current (CC) and constant voltage (CV) charging, which are performed by DC/DC converters [33]. A block diagram of the fast-charging system configuration is shown in Figure 4. The control algorithms used for the charging mode operation of the power control unit include proportional–integral (PI) control, proportional–integral–derivative (PID) control, sliding-mode control, and neural network control [34].

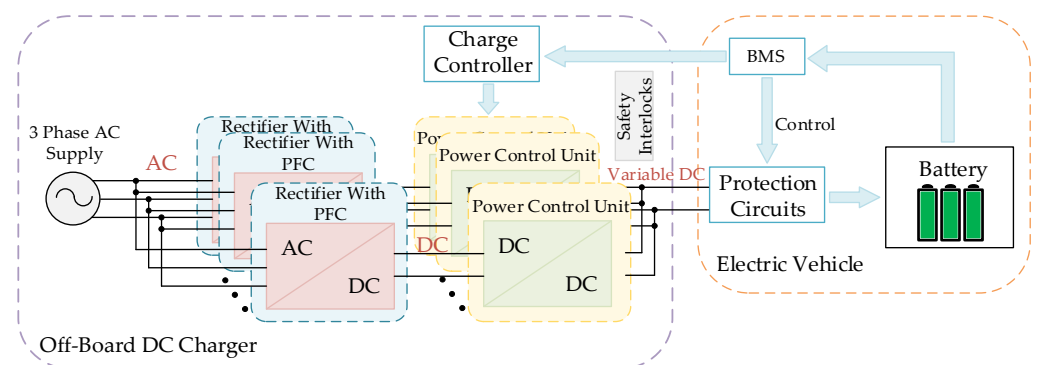


Figure 4. Block diagram of the configuration of the fast-charging system.

According to IEEE Standard 1547 [35], electrical isolation between the grid and the EV power cell can be provided by a low-frequency transformer or a high-frequency transformer inside the isolated DC/DC converter. The electrical isolation allows the power modules to be connected in parallel. If a single module cannot meet the power requirements of a fast-charging system, connecting multiple identical modules in parallel can increase the output power. The Tesla supercharger uses 12 groups of modules connected in parallel to output power. The topology and control algorithm of the fast-charging system are described in Sections 4–7 of this paper.

3. Charging Interface and Technical Specifications

The charging interface is an essential component that connects EVs to power supply equipment during the charging process. With the industrialization and globalization of EVs, there is a challenge of unifying charging interface standards across various countries, which hinders the ability to achieve charging interconnection between various types of EVs in different regions. In this case, regions such as China, the United States, Europe, and Japan actively promote the unification of charging interface standards [36]. The standardization of EV charging interface standards is crucial in promoting and encouraging the widespread adoption and use of EVs and in facilitating the development of the charging infrastructure. Currently, there are several global standards for EV charging interfaces, including the

IEC standards [37], CCS joint charging standards [38], CHAdeMO standards [39], SAE standards [28], GB/T standards [40], etc.

According to SAE J1772, based on their power levels, EV charging systems can be classified into Level 1, Level 2, Level 3, and ultra-fast-charging. Level 3 and ultra-fast charging systems directly provide power to the EV battery at levels of 350 kW or higher. Ultra-fast-charging systems can recharge a battery to a 300 km driving range in 10 min or less [41]. The current fast-charging interfaces used worldwide are shown in Figure 5.

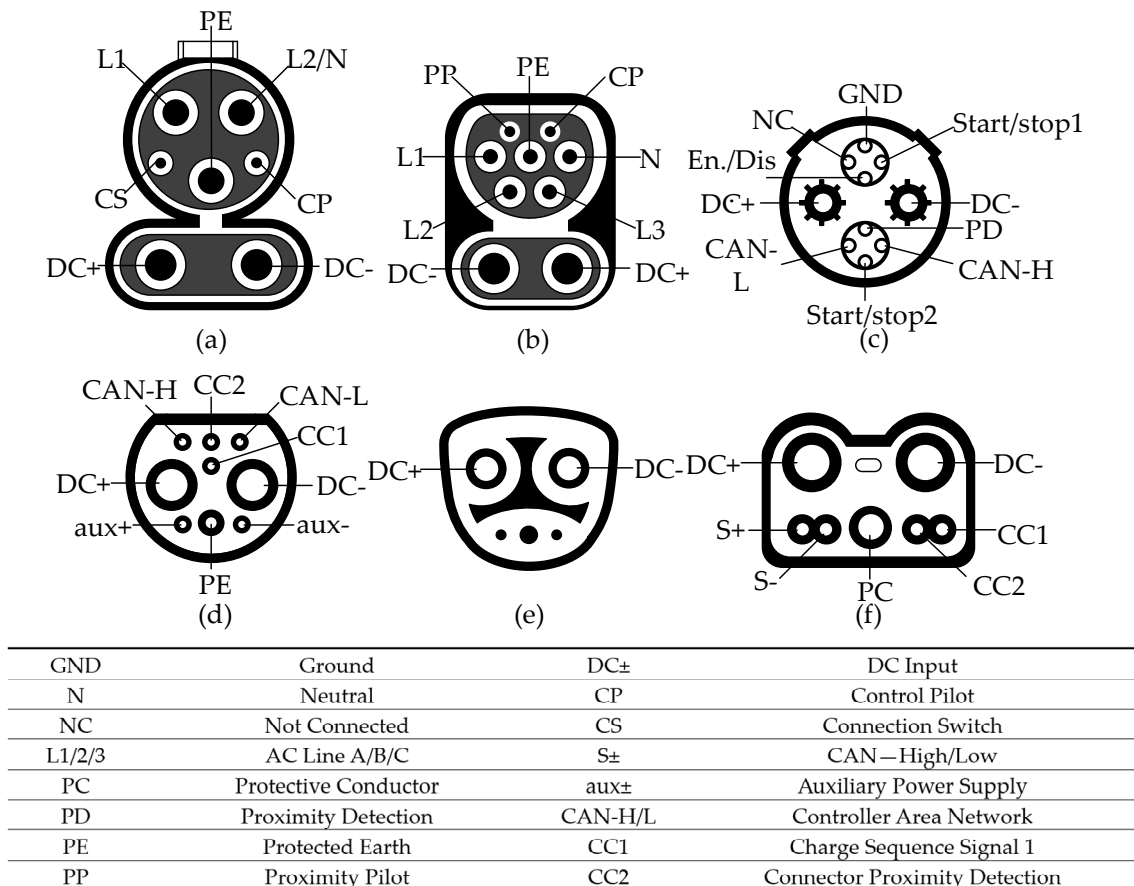


Figure 5. Current global fast-charging interfaces. (a) CCS Combo 1; (b) CCS Combo 2; (c) CHAdeMO; (d) GB/T 20234.3; (e) Tesla Supercharger; (f) CHAdeMO 3.0/Chaoji.

The CCS Combo 1 interface shown in Figure 5a was released by SAE International in October 2012. It is mainly used in North America and is compatible with the SAE J1772 interface used in the U.S. and Japan, with a maximum voltage of 600 V, a maximum current of 200 A, and power of up to 150 kW. The CCS Combo 2 interface shown in Figure 5b is an upgrade of the CCS Combo 1 interface, which was jointly launched in 2012 by eight European and American manufacturers, including Audi, BMW, Ford, and Chrysler, to enable high-power charging. The system can currently support a maximum voltage of 1000 V, a maximum current of 400 A, and power of up to 350 kW [38]. The CHAdeMO charging interface shown in Figure 5c is mainly used by Japanese car companies, which released the CHAdeMO version 1.2 and 2.0 standards in 2017 and 2018 that support power outputs of up to 200 kW and 400 kW [39]. The GB/T 20234.3 interface shown in Figure 5d represents the charging interface standard of China. This interface uses the CAN bus communication protocol with a rated current of no more than 250 A and a theoretical power of 250 kW [40]. Car companies represented by Tesla use charging interfaces independent of each standard series that are mainly applied in the U.S., as shown in Figure 5e. This charging interface currently has a maximum power of 250 kW, maximum current of 600 A,

and maximum voltage of 400 V. The CHAdeMO 3.0/Chaoji charging interface shown in Figure 5f was jointly developed by the China Electricity Council and CHAdeMO to promote the technical research and development of international standards for high-power field charging [42]. On June 19, 2020, the "White Paper of Chaoji EV Charging Technology" and CHAdeMO 3.0 standards were announced. The maximum output power of this charging interface is 900 kW, the maximum current is 600 A, the maximum voltage is 1500 V, and there is a maximum charging time of 5 min for a 400 km driving range. At the same time, due to Chaoji's compact design and scalability, it can be expanded to small and medium power applications. The Chaoji charging system can adapt to ultra-high power, addressing the long-standing issue of the short range and long charging time of EVs. As a result, it has a wide range of application prospects. The types of charging interfaces and their electrical characteristics are shown in Table 3. The continuous optimization of charging interfaces also promotes the development of high-power charging technology.

Table 3. Electrical characteristics of global high-power charging interfaces.

Standard	Maximum Voltage/V	Maximum Current/A	Maximum Power/kW
CCS Combo 1	600	200	150
CCS Combo 2	1000	400	350
CHAdeMO	1000	400	400
GB/T 20234.3	1000	250	250
Tesla Supercharger	400	600	250
CHAdeMO 3.0/Chaoji	1500	600	900

4. Front-Stage AC/DC Converter Topologies

To meet the fast-charging requirements of EVs, the front AC/DC converter typically uses a three-phase high-power rectifier. This section introduces the three common topologies and analyzes their technical features in detail: three-phase boost-type rectifier, three-phase buck-type rectifier, and multilevel rectifier topologies.

4.1. Three-Phase Boost-Type Rectifier Topologies

The three-phase six-switch boost rectifier (TPSSBR) has the advantages of a simple structure, high efficiency, a high power factor, low total harmonic distortion (THD) of the input current, low current stress, low cost, and bidirectional energy flow capabilities. The topology of the TPSSBR is shown in Figure 6a. Each bridge leg of the TPSSBR consists of a field-effect transistor, and the parasitic diode of the field-effect transistor can provide a freewheeling path for the inductor current in the dead time to realize a continuous input current. The output voltage of the TPSSBR is higher than the peak value of the AC input line voltage, therefore, the components need to withstand higher voltage stress and the requirements for the rear-stage converter to withstand voltage are correspondingly higher. In addition, the input voltage is directly connected to the DC-side capacitor through the parasitic diode, which can lead to large inrush currents at the moment of startup. When a short-circuit fault occurs in a bridge leg, it can cause an instantaneous overcurrent in the rectifier, resulting in damage to the power components. The TPSSBR is widely used in EV charging systems. In [43,44], a TPSSBR was proposed that can realize charging operations while regulating the grid voltage and correcting the power factor. In [45], a SiC-based 200 kW ultra-fast-charging system was designed, which achieved an overall operating efficiency of higher than 98.5% and a total input current distortion of less than 2.2%. Moreover, this system can provide reactive power support to the grid. The converter proposed in [46] was composed of two TPSSBRs in parallel, which can control the grid current and DC-link voltage. This structure can effectively reduce the current flowing through the power components and reduce the size of the passive filter and the harmonic content of the grid current. To further improve the efficiency of the converter, an auxiliary resonant branch

composed of an auxiliary active switch, resonant inductor, and clamping capacitor was added to the traditional TPSSBR in [47]. The proposed space-vector modulation strategy enables the turning on of all main and auxiliary switches under zero-voltage conditions, the elimination of the reverse recovery current of the diode, and the equalization of the voltage stress of all switches with the DC-link voltage.

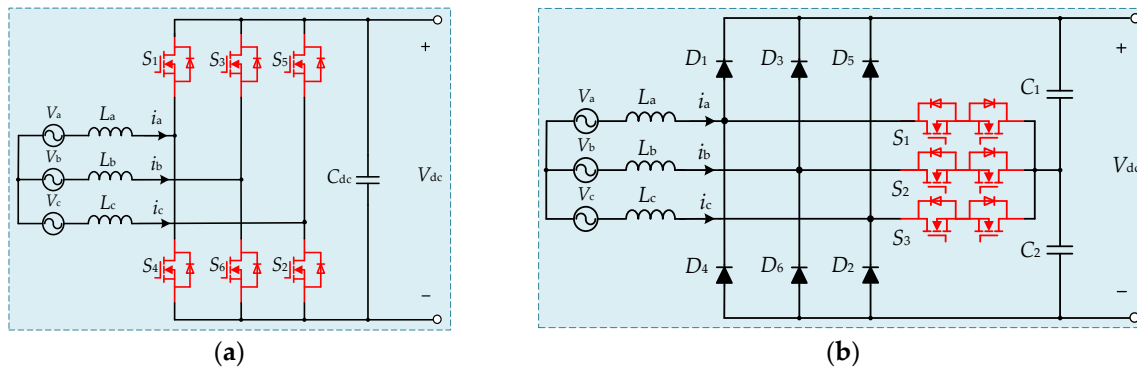


Figure 6. Three-phase boost-type rectifier topology. (a) Three-phase six-switch boost rectifier. (b) Vienna rectifier.

The Vienna rectifier is a three-phase boost-type three-level rectifier and its topology is shown in Figure 6b. Each phase bridge leg has a bidirectional switch, which is composed of two power components in series. When the bidirectional switch of a certain phase is on, the phase is connected to the neutral point of the output capacitor side, and when the bidirectional switch of a certain phase is off, the current can flow through the diode on the bridge leg. Compared to the TPSSBR, the Vienna rectifier does not have the advantage of shoot-through and does not need to consider the dead-time problem, therefore, it is more reliable but its energy can only flow in one direction. In addition, the Vienna rectifier inherits some advantages of the three-level rectifier due to the reduced number of switches. The Vienna rectifier switches operate under lower voltage stress, which is only half of the output DC voltage. This results in lower switching losses and less conducted electromagnetic interference (EMI) noise [48]. Moreover, the lower harmonic content of the input current reduces the size and cost of the input-side filter inductor and increases the power density. However, the Vienna rectifier also has the problem of unbalanced voltage at the neutral point of the output capacitor on the DC side. The fluctuation of the neutral-point voltage increases the voltage stress of the switch and causes harmonic distortion of the input current. The authors of [49–51] addressed this problem and provided relevant solutions. The Vienna rectifier has been applied in high-power charging systems by many enterprises. In [52], different Vienna topologies were compared based on the number of components, efficiency, THD of the input current, and power factor. In [53], a Vienna rectifier based on a digital multi-loop control strategy was proposed, which can achieve an ultra-fast charge of 30 kW. In [54], a Vienna rectifier based on a voltage-oriented controller was proposed, which guarantees a minimum ripple and distortion in the input sinusoidal current, reduces the requirements for the filter, and has a high power factor. With the application of wide-bandgap semiconductors and the optimization of passive components, the efficiency and power density of rectifiers are also improving. In [55], the loss and volume of the inductor were optimized based on the use of SiC components. The rectifier efficiency reached 98% at rated power and the power density reached 2.3 kW/L. In [56], zero-voltage switching (ZVS) for all transition processes was achieved by improving both the topology and modulation, further reducing power losses.

4.2. Three-Phase Buck-Type Rectifier Topologies

The topology of the three-phase buck rectifier (TPBR) is shown in Figure 7a. Because the input current of the TPBR is intermittent during each switching cycle, an LC filter

is required to filter out the high-order harmonics in the input current [57]. Each phase of the TPBR bridge leg is composed of a switch and a diode in series, which ensures a unidirectional flow of the current in the bridge leg and improves the reverse voltage resistance of the switch; however, it also results in large conduction losses [48]. Compared to the TPSSBR, when all the switches of the TPBR are turned off, there is no power flow path so the TPBR has a lower starting current [58]. In addition, the output voltage of the TPBR is lower than the peak AC input line voltage, allowing for a wider range of the output voltage regulation and less voltage stress on the power supply equipment cascaded with it. The energy storage inductor at the output side can restrain the short-circuit current, improve the reliability of the system, and realize the stability of the output current at the DC side. In [59], a typical TPBR design scheme was proposed, the loss calculation model for each component was discussed, and the efficiency of the optimized rectifier reached 98.8%. In [60], a converter consisting of two phase-shift-modulated six-switch TPBRs in parallel was proposed, which achieved higher efficiency and lower input harmonic current distortion. In addition, the use of SiC components in a TPBR allows for an increase in the switching frequency, which can reduce the weight and size of the output inductor. Lower switching losses can also lead to higher efficiency, but this can result in higher costs [61]. In [62], the three legs of the rectifier were delta-connected on the AC input side. This structure allows the DC-link current to be shared by more switches, which reduces the conduction losses by 20% and the current stress on the components. In the charging system, the voltage stress of power components is a problem that cannot be ignored. Although IGBT has a high-rated voltage, its switching performance is poor when it operates at high frequencies, whereas the MOSFET has a high on-resistance when the voltage is high, which can affect efficiency. Therefore, an improved scheme was proposed in [63]. By replacing the freewheeling diode with two diodes in series and connecting the input neutral point to the common point of the two diodes, the switch only needs to withstand the phase voltage. Based on this, low-voltage stress was also achieved in [64] by connecting the two output capacitors in series and adding a small capacitor between the input neutral point and common point. In [65], a novel voltage clamp three-phase two-switch Buck PFC circuit was proposed, which effectively reduces the voltage stress on the switches while retaining the advantages of simple control.

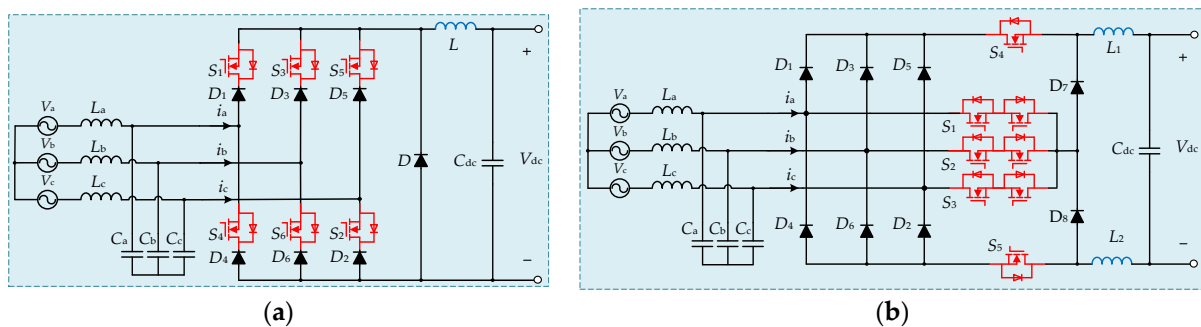


Figure 7. Three-phase buck-type rectifier topology. (a) Three-phase six-switch buck rectifier. (b) Swiss rectifier.

The Swiss rectifier is a new three-phase buck rectifier, which consists of an input filter, a three-phase diode rectifier bridge, two buck converters connected in series with the output of the rectifier bridge, and a third harmonic injection network. Its topology is shown in Figure 7b. The three bidirectional switches of the third harmonic injection network operate at twice the input voltage frequency, resulting in lower switching losses and higher efficiency compared to the three-phase six-switch Buck rectifier [66]. The Swiss rectifier can operate at a unity power factor and has the advantages of a low harmonic distortion rate of the input current and a wide range of output voltages, making it suitable for EV charging systems. In addition, the Swiss rectifier does not require the current space

vector pulse-width modulation strategy so its control is simpler [67]. The disadvantage of the Swiss rectifier is its relatively high number of switching components, which is not conducive to low costs or a high power density. In [68], a parallel Swiss rectifier based on an interleaved switching strategy was proposed. The switching frequency can be doubled to reduce the filter size but its application is limited due to the double number of components. The authors of [69] addressed this issue by only interleaving the buck circuit. In addition, the efficiency was significantly improved by using fewer components. In [70], a Swiss rectifier with interleaved output stages was proposed and the DC output inductance was optimized. This structure reduces the ripple of the input current and voltage and improves the THD of the input current, achieving a 99.3% efficiency. In [71], a single-stage isolated Swiss rectifier based on a single full bridge with a midpoint clamper was proposed, which utilizes only one full-bridge structure, reduces the conduction loss of the switches, improves the core utilization, and realizes electrical isolation and the soft-switching function. In [72], the DAB converter and Swiss rectifier were combined to realize the functions of PFC and soft switching, achieving low input current distortion and bidirectional power flow.

4.3. Multilevel Converter Topologies

Compared to the two-level converter, the multilevel converter can significantly improve the waveform of the input voltage and current. Under the same switching frequency, the current harmonics are smaller, thus reducing the filter inductance on the grid side to reduce the volume of the rectifier and effectively improve the power density. Due to the increase in the level number, the voltage change rate, EMI, and switching loss are reduced, and the voltage borne by the switch when it is turned off is also smaller, making it suitable for use in EV charging systems [73,74]. However, the multilevel converter also has inherent disadvantages, that is, the number of required power components increases with the increase in the number of levels, and the structure and control of the circuit become more complex. According to their circuit structure, multilevel converters can be divided into neutral-point-clamped (NPC) [74–76], flying capacitor (FC) [77,78], and cascaded H-bridge (CHB) [79–81] converters. The circuit topology is shown in Figure 8. For the NPC multilevel converter, when operating at high frequencies, the reverse recovery time of the diode limits the switching frequency of the converter. In addition, the conduction time of the switches in the middle of the bridge leg of the converter is different from that on both sides, which can lead to the inconsistent service life of each switch and cause different charging and discharging times of each DC capacitor, resulting in an unbalanced output voltage and affecting power quality. Therefore, a balancing circuit needs to be added, which increases costs and reduces efficiency [75,76]. To address the above issues, scholars proposed an FC multilevel converter, which uses a flying capacitor to replace the diode so that the voltage stress of the switch can be limited, and some capacitor voltage-balance strategies [77,78]. However, the increase in the number of capacitors also leads to an increase in the cost and volume, which can affect the power density of the system. CHB multilevel converters combine multiple identical H-bridge units in a cascading manner to achieve higher output voltage by using power components with limited voltage resistance [79]. Its topology is simpler than the NPC converter and has the advantage of high modularity. It can increase or reduce the number of modules to adapt to the charging power, and the AC side of the system can output multiple levels to reduce the harmonic pollution of the power grid [80]. The DC capacity of each module in the system is self-contained, making voltage-balancing measures easier to realize. In [73], a megawatt-level modular multilevel converter based on three-level active-neutral-point-clamped cells in parallel was proposed, which requires only six high-frequency SiC switches operating at 333 kHz to generate a 1 MHz switching spectrum, thus significantly reducing switching losses. In [82], a power electronic transformer based on a multilevel converter was analyzed and reviewed in detail, demonstrating its potential for broad applications in EV charging systems.

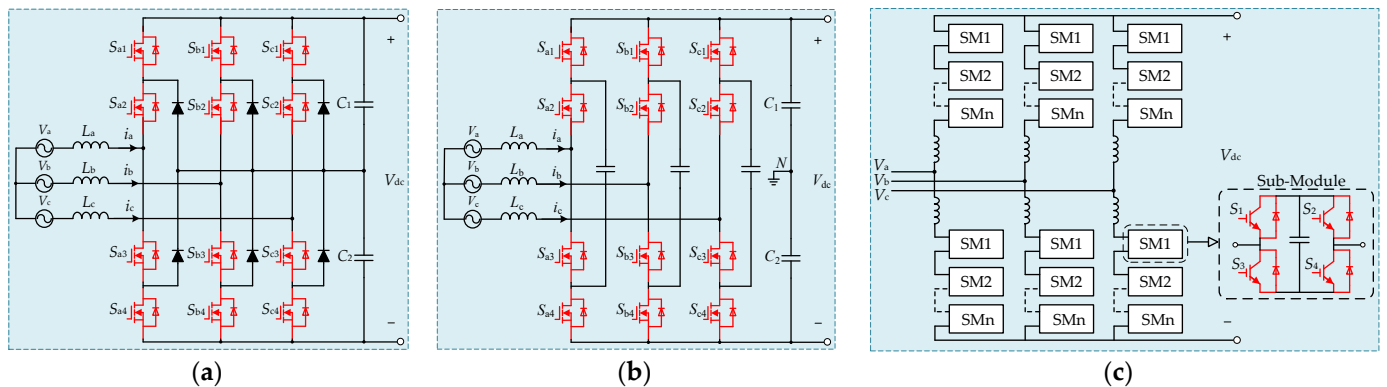


Figure 8. Multilevel converter topology. (a) Neutral-point-clamped three-level converter. (b) Flying capacitor three-level converter. (c) Cascaded H-bridge multilevel converter.

5. Rear-Stage DC/DC Converter Topologies

The rear-stage DC/DC converter is used to output a wide range of adjustable DC to adapt to the load characteristics of high-voltage power batteries for EVs. There are typically two architecture forms for these converters, namely non-isolated and isolated DC/DC converters.

5.1. Non-Isolated DC/DC Converter Topologies

Non-isolated DC/DC converters are simpler, have lower losses, and are more efficient because they do not use isolation transformers. In [83], a step-down/step-up bidirectional converter suitable for V2G and Grid to Vehicle (G2V) was proposed. The circuit has a wide voltage gain range, which can realize the dynamic matching between the battery voltage and the constant DC bus voltage. In [84], a multi-phase interleaved DC/DC converter was proposed. As shown in Figure 9a, it works as a buck converter in the charging mode operation of the battery and the boost mode operation during the discharging of the battery. Due to the small size of the inductor, the interleaved operation of the converter helps to control the charging current under different charge states. In [85], a non-isolated bi-directional DC/DC converter with multi-phase interleaved half-bridge topology was proposed. The coupled output inductor is used to reduce the current ripple but it has inherent voltage-balance limitations. In [86], a multi-phase interleaved buck converter was proposed. The converter has a variety of characteristics, including current sharing, a lower output capacitor current ripple, better heat distribution, and smaller filter and radiator sizes. It uses interleaving techniques to reduce the output current ripple and improves efficiency by distributing the power balance among the phases. In [87], a high-power three-level DC/DC converter was proposed, as shown in Figure 9b. The converter adopts two groups of parallel three-level structures to achieve a high power output. The topology is compatible with the bipolar DC bus structure and eliminates the balance circuit of the NPC AC/DC converter. However, in this working mode, if multiple charging systems work at the same time, there will be a high DC-link voltage ripple and circulation. To address this issue, a parallel three-level DC/DC converter with an integrated inductor structure was proposed in [88]. The inductor in the converter contains an integrated magnetic core with output and circulating windings for filtering the output current and reducing the circulating current. In [89], a topology of a three-phase buck converter connected in parallel was proposed to improve the DC bus voltage and charging power level. In [46], a bidirectional three-level asymmetric voltage converter was proposed, as shown in Figure 9c. Compared to the non-isolated DC/DC converter with a half-bridge structure, the current ripple is significantly lower. In [90], a non-isolated soft-switching bidirectional DC/DC converter with interleaved technology and a built-in transformer was proposed. The T-type neutral point clamping circuit is integrated into the traditional interleaved buck-boost converter to obtain a high-voltage gain ratio and effectively reduce the voltage stress of the

power switch. The interleaved structure can effectively reduce the current ripple on the low-voltage side and help to achieve voltage matching on both sides of the transformer under pulse-width modulation control while reducing the circulating current to improve efficiency.

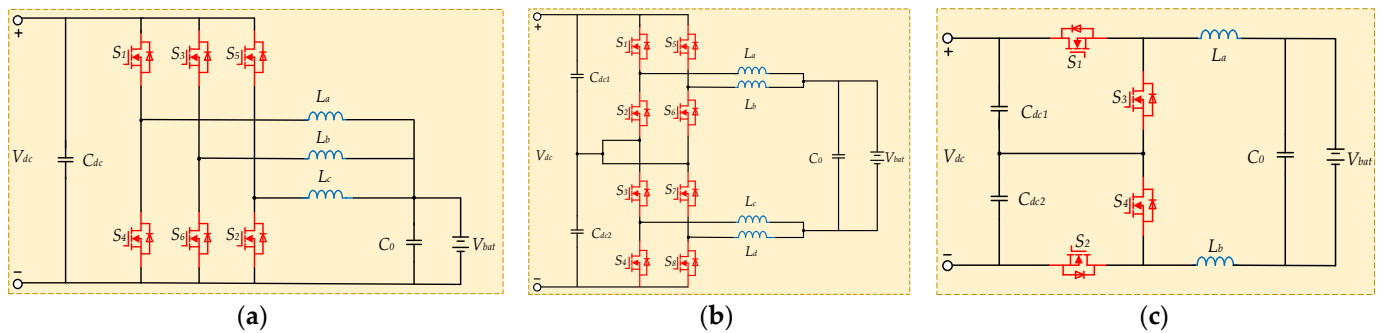


Figure 9. Non-isolated DC/DC converter topology. (a) Multi-phase interleaved DC/DC converter. (b) Three-level DC/DC converter. (c) Three-level asymmetric voltage converter.

5.2. Isolated DC/DC Converter Topologies

Isolated DC/DC converters for EV fast-charging systems can be divided into the following categories: resonant converters, DAB converters, and phase-shifted full-bridge (PSFB) converters [91].

The LLC resonant converter is widely used in high-voltage and high-power-density EV charging systems and its topology is shown in Figure 10a. The LLC resonant converter has attracted attention due to its high efficiency, high power density, low EMI, and wide voltage range. For lithium battery units, CC and CV charging are required. When the battery is in a CV or trickle-charging state, the light-load efficiency becomes an issue for the LLC resonant converter [92]. In [93], a novel dual full-bridge LLC resonant converter for CC and CV charging of EV batteries was proposed. One full-bridge LLC resonant converter is controlled by a fixed resonant network, whereas the other uses a variable resonant network for CC and CV charging operations. All switches in CC charging mode can achieve ZVS and zero-current switching (ZCS), and all switches in CV charging mode can achieve ZVS. A magnetically controlled dual half-bridge LLC resonant converter was proposed in [94]. Using interleaved parallel technology, two LLC resonant networks share the main switch and the output side is connected in series. One of the LLC resonant converters is designed to operate at a series resonant frequency, whereas the other LLC resonant converter uses magnetic control to adjust the total output current and voltage in CC charging mode and CV charging mode [95]. In [96], a full-bridge LLC resonant converter with series-parallel transformers was proposed and its topology is shown in Figure 10b. The converter can achieve the ZVS of the switch tube and the ZCS of the diode, as well as automatic power balance. The series connection can reduce the number of turns of the primary winding and the parallel connection can reduce the current stress of the secondary winding group and the conduction loss of the rectifier diode. In addition, the converter has the same advantages as the LLC resonant converter. In [97], an LLC resonant converter with a laminated structure, as well as a new control scheme, was proposed. The frequency multiplier modulation strategy is used to reduce the switching loss and driving loss, and the output is adjusted by frequency modulation.

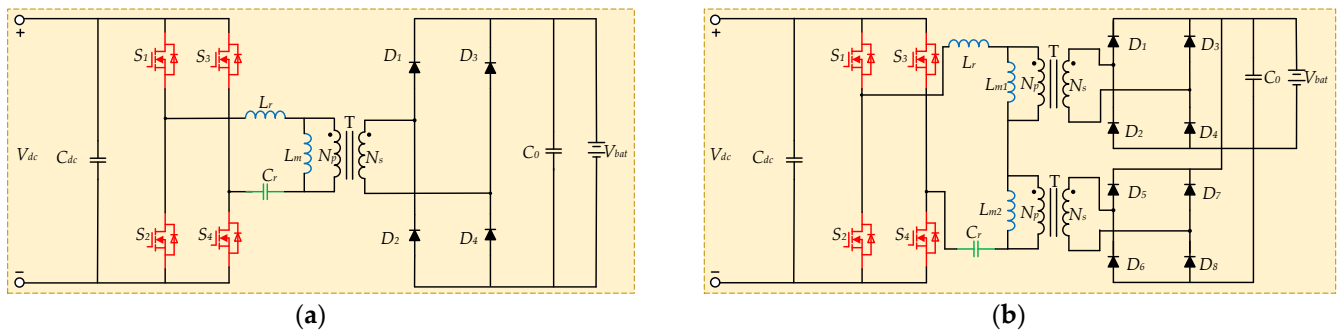


Figure 10. LLC resonant converter. (a) LLC resonant converter. (b) LLC resonant converter with series-parallel transformer.

The development of V2G technology will further accelerate the development of the EV industry. Therefore, bidirectional power flow, high power density, and high efficiency have become the main technical indicators of fast-charging systems [98]. The bidirectional CLLC resonant converter has the potential for use in EV charging systems due to its soft-switching and bidirectional power flow capabilities. The topology is shown in Figure 11. The traditional CLLC resonant converter typically adopts a symmetrical design to maintain the symmetrical characteristics of bidirectional energy flow. The symmetrical design is only suitable for applications that do not require a wide voltage range. Due to the wide voltage range of the battery, there must be characteristic differences between charging and discharging modes so a completely symmetrical topology cannot meet the application requirements. To address this issue, a CLLC design method based on parameter equivalence and a time-domain model was proposed in [99]. Based on the principle of parameter equivalence, a CLLC resonator with arbitrary parameters was designed to meet the requirements of a wide voltage range for bidirectional charging and discharging. An asymmetric parameter design method was proposed in [100]. The gain curves of charging and discharging modes were designed so that the switching frequency ranges of the two modes could overlap, thereby reducing the change in the bidirectional frequency range.

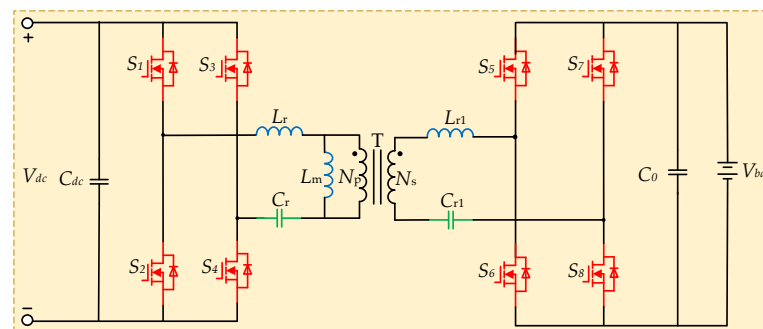


Figure 11. CLLC resonant converter.

The DAB converter can automatically adjust the bidirectional power flow, wide voltage gain range, and ZVS capability, and its topology is shown in Figure 12. The modular parallel connection of the DAB converter allows it to expand to a higher power level. However, this type of converter also has certain disadvantages. It has a large reactive current and a large electrical stress on the power element, which increases the loss of the power element [101]. In [102], the single-phase shift (SPS), double-phase shift (DPS), and three-phase shift (TPS) control methods were applied to the DAB converter to ensure that all power components could achieve ZVS throughout the operating range of the load. In [103], the causes of the circulating current and loss of ZVS were comprehensively expounded. The methods used to suppress the circulating current were mainly the hardware method and the duty-cycle method. The core idea was to control the equivalent voltage gain close to 1. In [104], a

sinusoidal charging scheme was proposed, which consists of a full-bridge AC/DC converter and a DAB converter. The influence of the converter loss on the ripple power balance was analyzed. On this basis, a feedback control method for the DC bus voltage ripple was proposed, which can control the charging curve more flexibly, thereby improving charging efficiency and battery life. In [105], a dual-band current control method for DAB converters was proposed to avoid the risk of transformer saturation. In [106], a transformer saturation suppression algorithm for DAB converters was proposed. By detecting the change in the transformer current slope near the saturation boundary and applying the duty cycle offset to the DAB converter, the transformer saturation was suppressed.

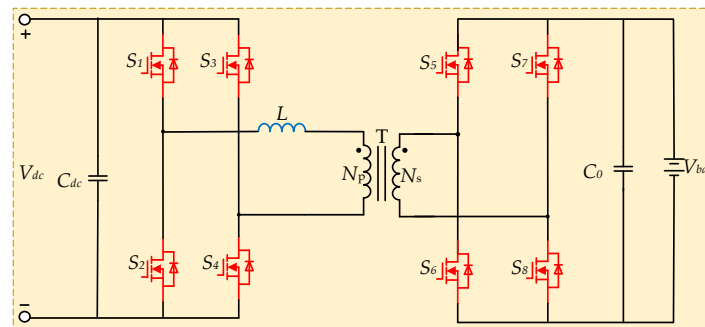


Figure 12. DAB converter.

The traditional PSFB converter has been widely used in EV charging systems. Its topology is shown in Figure 13. The main features of the PSFB converter are its simple circuit, high conversion efficiency, high power density, constant operating frequency, and low EMI. The PSFB converter can achieve ZVS, even without additional circuits. The main disadvantages of the PSFB converter are that the ZVS range of the lagging branch switch is narrow, and the circulating current, duty cycle loss, voltage oscillation, and reverse recovery current of the rectifier diode are relatively large [107]. In [108], a novel PSFB converter with a novel center-tapped clamp circuit was proposed. It uses two diodes and a capacitor to form a center-tapped clamp circuit, which addresses numerous issues in traditional PSFB converters. In [109], a novel interleaved current-driven PSFB converter was proposed. The converter has a voltage-doubler rectifier, and the power element can achieve ZVS in a wide load range, which can eliminate the voltage spikes at both ends of the secondary rectifier, and the output diode is non-destructively commutated due to the current-driven mode. In order to improve the performance of the traditional phase-shifted full-bridge pulse-width modulation converter, an improved zero-voltage zero-current switching phase-shifted full-bridge pulse-width modulation converter was proposed in [110]. By adding a simple auxiliary circuit, the leading branch switch realizes zero-voltage switching and the lagging branch switch realizes zero-current switching. During the freewheeling period, the primary current is reset, thereby improving the efficiency of the converter. In addition, the improved converter can effectively reduce the output current ripple. In [111], an improved control method for the PSFB converter was proposed. By adjusting the phase-shift angle between the primary side and the secondary side of the circuit and the duty cycle of the secondary side, the pre-charging stage and the co-charging stage are added to address the issues in the bidirectional PSFB converter. Compared with DAB and CLLC converters, the PSFB converter has a lower root-mean-square current, which minimizes the current stress and conduction loss [112]. The dynamic response of the PSFB converter is superior to other topologies. Because its output gain is related to the phase angle and works at a fixed switching frequency, the PSFB converter is more suitable for applications with frequent bidirectional energy flow. However, since the PSFB converter can only achieve hard switching on the secondary side, the switching loss of its power components is higher than that of resonant topologies such as CLLC. In [113], an asymmetric pulse-width modulation full-bridge converter with ZVS and a reduced circulating current was proposed. To reduce the circulating current, an

improved PSFB converter with asymmetric pulse-width modulation control was adopted. The converter has a split capacitor and an improved rectifier. All switches can achieve ZVS and reduce the output current ripple.

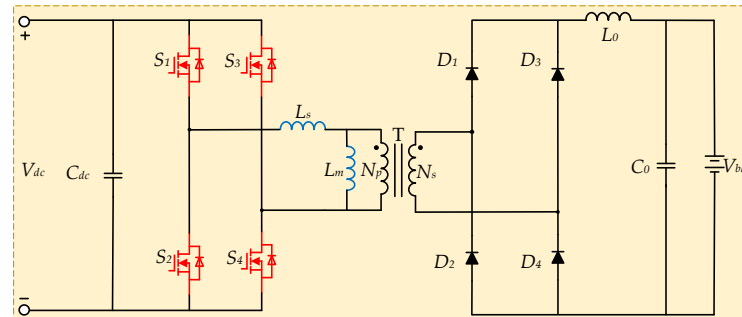


Figure 13. PSFB converter.

6. Front-Stage AC/DC Converter Control Technology

This section discusses the control strategies of various AC/DC converters in terms of control objectives, control methods, and common problems.

6.1. Three-Phase Boost-Type Rectifier Control Technology

The control objectives of the three-phase boost rectifier mainly consist of two parts: (1) ensuring a stable and reliable output voltage at the DC side; and (2) achieving unity power factor operation by keeping the voltage and current of the AC side of the rectifier in the same phase. To achieve this, the dual-loop control method is typically adopted for the voltage outer loop and current inner loop. The voltage outer loop is responsible for controlling the output voltage of the DC side and providing a reference current for the inner-loop control. In [114], the control system was composed of a dual-loop voltage-current controller. Four different types of controllers, PI, lead-lag, proportional-resonance (PR), and modified proportional-resonance controllers, were used for the current loop, and the performance of the voltage ripple and current THD under different conditions was compared. Taking the design of the PI controller as an example, the author first established a linear model of the system in the form of the state space. After closed-loop analysis, the PI controller was optimized according to the margin and frequency. The inner-loop current PI controller was designed at $< 1/10$ of the switching frequency and the outer-loop voltage control was designed at a 50 Hz line frequency. The control performance was optimized by adjusting the control gain to obtain the appropriate overshoot, undershoot, rise time, and settling time. In addition, there are other studies that use the MATLAB toolbox and experiments to determine the PI parameters. However, the sampling time delay is inevitable in the traditional PI controller due to the error-tracking method. In contrast, model predictive control can predict the value of the next sampling period based on the system model. In [115], the finite set-model predictive control (FS-MPC) algorithm was used, which uses the discrete behavior of the converter to determine the appropriate switching states that minimize the cost function. This method achieved bidirectional power transfer with instantaneous mode-changing capabilities and a fast dynamic response. In [116], continuous control set-model predictive control was adopted, which can realize a fixed switching frequency and reduce the computational burden, in addition to having a better dynamic response and robustness. In addition, direct power control in a smart power grid can better regulate the active and reactive power of the system, which is conducive to the energy exchange between the V2G system and the power grid. In [44], a direct power-control method based on dual loops was proposed, which can adjust the grid current and charging current by receiving a command from the active power or reactive power, achieving a fast response speed. In [117], a control system consisting of an outer voltage loop and an inner deadbeat instantaneous power loop was proposed, which can realize

the fast-tracking of instantaneous power and bidirectional energy flow. In [118], a droop control strategy was proposed to optimize the converter, which can adjust the frequency deviation in the distribution feeder by controlling the bidirectional active power and the charging and discharging processes.

The Vienna rectifier typically adopts a dual-loop control strategy. The voltage outer-loop control is relatively simple, whereas the current inner-loop control is more complicated due to the sinusoidal input current and PFC. Many control strategies are applied to Vienna rectifiers, including PR control [49,119], voltage-oriented control [54], model predictive control [120,121], one-cycle control [122], and sliding-mode control [123], among others. Neutral-point voltage fluctuation is an inherent problem in Vienna rectifiers. To address this, a dual-loop hybrid control scheme was proposed in [121] and its control block diagram is shown in Figure 14. The outer loop uses a PI controller to regulate the DC-link voltage and input reactive power. The output of the controller is used as the active current reference i_d^* , and the reactive current reference i_q^* is determined by the reactive power requirements and is then converted into an expression in $\alpha\beta$ coordinates. The inner loop uses FS-MPC to regulate the input current to maintain the neutral-point voltage balance. i_a^p and i_b^p are the predicted input current, u_1^p and u_2^p are the predicted capacitor voltage, \hat{i}_o is the estimated load current, and finally, the combination of switching states (S_1, S_2, S_3) is obtained. This scheme has good dynamic performance and a wide operating range but it also has the disadvantage of an unfixed switching frequency. In [122], the neutral-point voltage balance control loop was added based on one-cycle control, which can eliminate the neutral-point voltage fluctuation and improve the voltage utilization rate of the DC-link. In [124], a harmonic resonance suppression strategy based on the impedance matching principle was proposed, which can not only ensure the low ripple output voltage of the Vienna rectifier but also suppress the background harmonic resonance amplification to effectively improve the power quality of the Vienna rectifier's grid-connected current and common coupling point voltage.

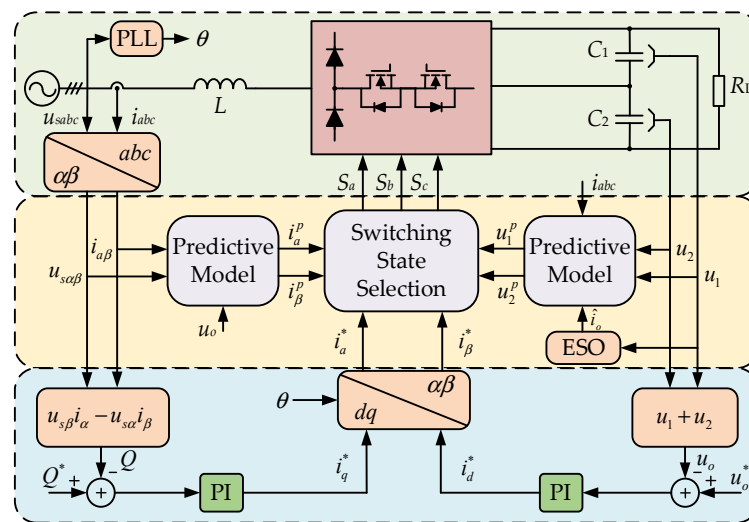


Figure 14. Control block diagram of Vienna rectifier.

6.2. Three-Phase Buck-Type Rectifier Control Technology

Based on whether the input current is detected, the control technology of the TPBR can be divided into direct current control [125] and indirect current control [126,127]. Direct current control technology has a fast dynamic response and strong robustness to circuit parameters. Indirect current control has the characteristics of a good steady-state performance, simple control structure, and low cost but this method is more dependent on the system parameters. In [125], feed-forward decoupling and active damping control strategies were adopted, and the system achieved good dynamic and static performance

and low grid-side current harmonic distortion by optimizing the zero position and loop gain of the inner-loop controller. The proposed current outer-loop controller can effectively suppress the influence of the operating point of the system on its performance. In [126], a reconstructed phase-voltage-based power following control for the three-phase buck rectifier under unbalanced input phase voltages in a wide AC input frequency application was proposed. This strategy can make the input current more balanced and sinusoidal, and it can be easily implemented using digital control techniques. In order to suppress the harmonics of the input current and output voltage under the condition of AC input unbalance, a simple transfer-matrix digital control strategy was proposed for a three-phase six-switch buck rectifier [127]. The control block diagram is shown in Figure 15. The control strategy does not need to sample the input current but only needs to sample the input voltage V_a, V_b, V_c ; output voltage V_o ; and DC-link current i_L . The output of the inner current loop u^* is multiplied by the calculated sampled input voltages y_a, y_b, y_c to obtain the transfer matrix σ . The three-phase input currents are reconstructed from the DC-link current i_L using the space vector pulse-width modulation (SVPWM) strategy, which can realize the sinusoidal input currents and ensure that the input currents are in phase with the input voltages. This strategy does not need a phase-locked loop and complicated calculation, and can effectively reduce the cost and volume of the digital controller. In addition, the influence of sector update delay on the input current distortion and switching loss of a three-phase six-switch buck rectifier was studied in [58] and a time-delay compensation method was proposed, which can reduce the THD of the input current and improve system efficiency.

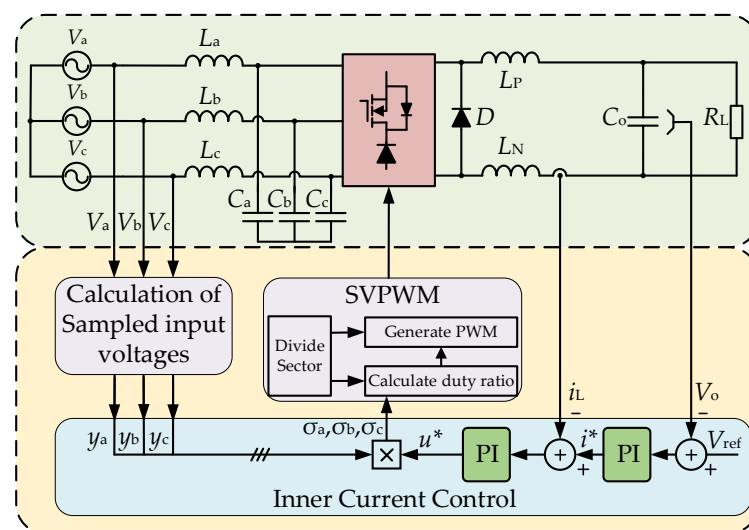


Figure 15. Control block diagram of three-phase six-switch buck rectifier.

For the Swiss rectifier, five different inner-loop feedforward options (constant voltage-transfer ratio, constant input current, constant output voltage, constant power transfer, and constant input resistance) were considered [128] and different schemes were analyzed and evaluated. Based on traditional PI dual-loop control, fuzzy PI control was introduced in [129] to achieve PFC, achieving better dynamic performance and robustness. Due to the switching frequency voltage ripple on the input filter capacitor of the Swiss rectifier, the input current of the three-phase diode rectifier bridge will commute frequently, resulting in a current distortion at the commutation boundary [130]. To address this, two control methods were proposed in [131]: one method was to allow the bidirectional switch to work in a high-frequency state near the commutation boundary so that the driving signal was complementary to the outer high-frequency switch; and the other method was to turn off the bidirectional switch near the commutation boundary to reduce the current distortion.

6.3. Multilevel Converter Control Technology

The control objectives of the three-phase multilevel rectifier mainly include three points: (1) controlling the output voltage of the DC side to improve the stability and dynamic response performance of the output voltage, and ensuring its ripple meets the design requirements; (2) balancing the capacitor voltage on the output side to avoid the abnormal operation of the system due to the unbalanced capacitor voltage; and (3) controlling the input current on the AC side to ensure that the input current and input voltage are in the same phase, reducing the THD and reactive power loss and achieving PFC. The current control strategy is the focus of the multilevel converter control strategy, which affects the operating frequency and transmission efficiency of the rectifier and determines the overall operating performance of the system. Currently, the main current modulation strategies of the multilevel converter are sinusoidal pulse-width modulation (SPWM) and space-vector modulation (SVM). In [74], PR control was adopted to effectively adjust the DC-link voltage and power factor. Based on phase-disposition SPWM, the system has bidirectional power flow capabilities and achieved good performance in both rectifier and inverter modes. In [75], in order to expand the controllable balance region and eliminate additional balance circuits, a voltage balance control (VBC) strategy for coordinating the NPC converter and DC/DC converter was established. The maximum available output current was utilized to achieve DC-link voltage balance and obtain a faster balance response. A coordinated VBC strategy also brings more freedom to grid-side current control and eliminates low-frequency fluctuations in the DC-link voltage. In [76], a voltage-oriented control scheme based on the SVM algorithm was adopted, and its control block diagram is shown in Figure 16. The control scheme uses four PI controllers. The top PI controller outputs Δ_s , which provides a reference for the redistribution of positive and negative small vectors to achieve precise control of the mid-point voltage. The PI voltage controller estimates the reference current signal i_{gd}^* by comparing the DC-link voltage V_d to the reference voltage V_d^* , and then obtaining the voltage control value V_{cd}^* through the inner-loop active current PI controller. The current PI controller of the reactive current loop regulates the power factor by managing the reactive current component i_{gq} . In [77], a capacitor voltage balance strategy based on closed-loop SVM was proposed. Based on the deviation of the capacitor voltage, the cost function is defined and minimized and the appropriate redundant switch state is selected in the available switch state. Using the SVM switch-state redundancy regulates the capacitor voltage to a reference value, and this strategy does not have any adverse effect on the harmonic distortion of the AC-side voltage. In [79], the decoupled current method was used, which allows for the independent control of active and reactive power by controlling the i_d and i_q current components, respectively. In [132], a unified VBC strategy was proposed, which can realize the voltage balance of the CHB DC-link under different power-flow directions, meeting the requirements of active and reactive power on the grid side through a d–q decoupled power controller. In addition, the output voltage of the CHB is susceptible to errors due to the nonlinear behavior of the electronic components. Therefore, a nonlinear compensation technique based on predictive current control was proposed in [133], which can greatly improve the harmonic content of the grid current under steady-state conditions within a single fundamental cycle.

Rectifiers are generally controlled using a double-loop control method that includes a voltage outer loop and a current or power inner loop. The current or power inner loop is commonly known as current closed-loop control or power closed-loop control. Some new control methods have been derived based on these two control approaches. In the double closed-loop control process, the outer loop is required to have good robustness and strong anti-interference and the inner loop is required to have a fast dynamic response. For the modulation technology of rectifiers, SPWM and SVPWM methods are generally used, but it is also necessary to consider the circuit topology, switching frequency, complexity of the algorithm, as well as other aspects, to make a reasonable choice.

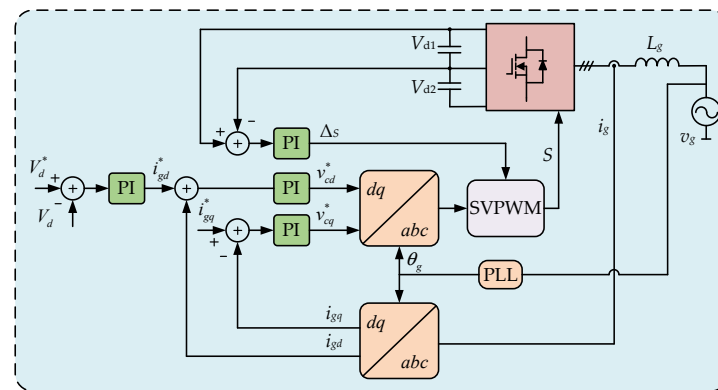


Figure 16. Voltage-oriented control block diagram of the three-level converter.

7. Rear-Stage DC/DC Converter Control Technology

This section discusses the control strategies of various DC/DC converters in terms of control objectives, control methods, and common problems.

7.1. Non-Isolated Converter Control Technology

The main control objective of the interleaved converter is to balance the interphase current, which aims to reduce the total current ripple and avoid power imbalance, thereby increasing the overall efficiency. At present, EV fast-charging systems require minimizing the current ripple of the input battery as much as possible to extend battery life. The control method proposed in [134] provides a wide range of battery voltages and a ripple-free battery current. In [85], a control method was proposed for lithium polymer batteries and lithium-ion batteries to meet the long life and safe operation requirements of these two types of batteries. In [89], to manage the power flow of the battery during charging and discharging, two cascaded PI controllers were used to control CC mode and CV mode. In [135], DC/DC converters achieved ZCS of all power devices at any voltage ratio of the high-voltage side voltage to the low-voltage side voltage. The bipolar DC bus feed charging system based on an NPC converter has many advantages. In [87], a fast-charging method with DC power balance management capabilities was proposed, which does not require the addition of extra balance circuits and high-frequency transformers, thereby improving the overall efficiency of the system. The fast-charging control method with comprehensive DC power balance management is shown in Figure 17. The upper-left box represents the output voltage and current control, where the charging profile (CP) provides the reference current i_{o2}^* , the reference voltage v_o^* , and the switch signal s_c to control the transition between CC charging mode and CV charging mode. Then, as the two units share the total output current, the current reference of each unit is set to $i_o^*/2$ and the four output currents of the two converter units are controlled using four PIs. Then, the outputs of the PIs are divided by the total input voltage $2v_i$ to generate the original modulation signals \bar{d}_{x1} , \bar{d}_{x4} . The lower-left box shows the comprehensive DC power balance management. In [75], a new VBC method was proposed, which expands the controllable balance region using the VBC method, thus eliminating the additional balance circuit. In [136], a model predictive control method was proposed, which integrates the internal and external dynamics of the DC/DC modular multilevel converter into the model predictive control algorithm and introduces three control objectives. Compared to the traditional PI control, the proposed model predictive control method reduces the AC circulating current in steady-state operation and has a faster response speed. In [137], a control technology based on harmonic elimination was proposed, which allows for the minimization of the ripple under asymmetric conditions.

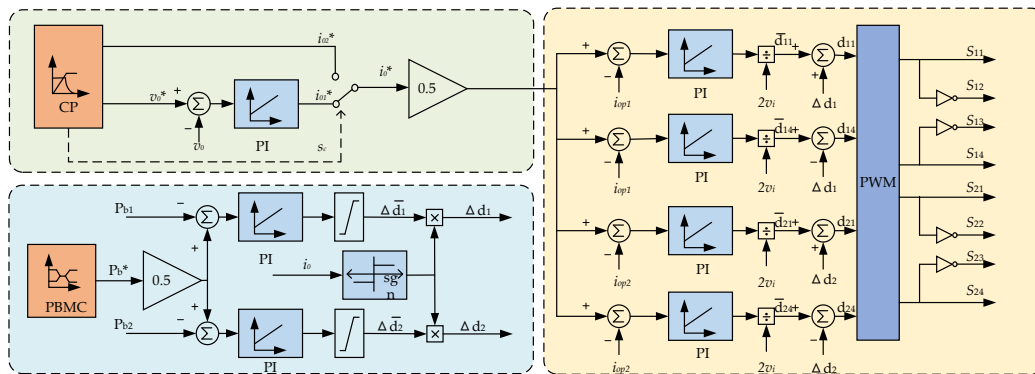


Figure 17. Fast-charging method with comprehensive DC power-balance management.

7.2. Isolated Converter Control Technology

The LLC converter has many advantages. However, during the process of EV charging, improving the working efficiency of the LLC converter under a light load is one of the key problems in this research area. In [138], a hybrid control method with adjustable frequency and a duty cycle was proposed, which can improve the performance of the full-bridge series-resonant DC/DC converter in CV charging mode. Compared to the conventional control method without any additional hardware, this control method can improve the efficiency of the charging system by 4% under light load conditions. At the same time, a new burst-mode control method was used to improve the light-load efficiency [139]. In [140], a burst-mode control method based on a simplified optimal trajectory was proposed to improve the efficiency of light loads. In [141], a hybrid-mode pulse-frequency modulation control method was proposed, which can achieve a fast dynamic response without an additional slope compensation circuit and can better adjust the output voltage without jump mode under light loads. The hybrid control strategy of pulse-frequency modulation and pulse-width modulation can significantly increase the adjustable output voltage range and perform sensitive automatic adjustments when the load conditions change while maintaining a stable target output voltage value [142]. This hybrid control strategy can also overcome the limited-frequency resolution problem [143]. A new control method for a full-bridge LLC resonant converter was proposed in [144]. Frequency control was used to adjust the output voltage under full-load conditions. By analyzing the loss of all power components, the optimal duty cycle was determined to obtain the minimum power loss under each light-load condition. In [93], the resonant tank parameters were designed to realize CC and CV mode charging at a fixed switching frequency and simultaneously realize soft switching. It adopts a simple PI control scheme, which consists of a PI controller, mode conversion switch, and limiter. When the battery voltage is lower than the maximum charge voltage, the current controller is activated to charge the battery with a constant current. Once the battery voltage reaches its maximum charge voltage, the controller automatically switches to CV mode by enabling the switch S mode and activating the voltage controller. The control block diagram is shown in Figure 18. In [145], the output voltage was adjusted using frequency conversion control. When the output voltage is high, the secondary winding group is in series. When the output voltage is low, fixed-frequency phase-shift control is used to adjust the configuration of the secondary winding group.

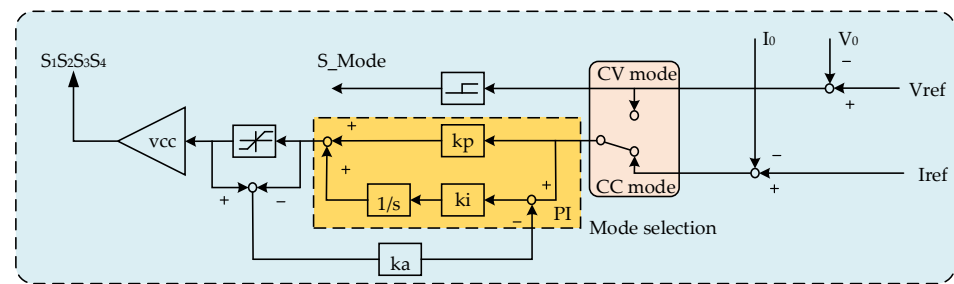


Figure 18. Closed-loop control method of the converter.

Scholars have described the small-signal modeling method and discrete-time average modeling method of the DAB converter in detail to analyze its dynamic characteristics. There are three techniques used to improve the dynamic performance of the DAB converter, including load-current feedforward control, direct inductor current control, and power-based control [146]. Based on state-space average modeling and small-signal modeling of the DAB converter, a model-based phase-shift control method was proposed in [147] to improve the dynamic characteristics of the DAB converter under load disturbances. In [148], by establishing a linearized dynamic model of the DAB converter, a load current feedforward compensation strategy was proposed to improve the output transient response of the converter under load disturbance conditions. In [149], a boundary control scheme using a natural switch surface was proposed to improve the dynamic characteristics of the system. Load current feedforward control is an alternative solution for improving the dynamic performance of load changes. Direct power control is an effective method to improve the dynamic response of the converter to achieve a fast dynamic response. In [150], a virtual direct power control scheme with fast response under complex conditions was proposed by combining direct power control with a feedforward control strategy. In [105], a dual-band current control method was proposed to avoid the risk of transformer saturation. In [151], a control scheme for a bidirectional isolated DAB converter based on sliding-mode control was proposed. This method not only achieves zero steady-state errors but also produces a fast transient response to load changes. Single-phase-shift modulation is the original modulation method of the DAB converter, but it is not enough to ensure the efficient operation of the DAB converter in the whole working range. Dual-phase-shift modulation is used to eliminate reactive power and improve system efficiency but it cannot achieve full-range soft switching. Three-phase-shift modulation provides a sufficient degree of freedom to extend the soft-switching range and reduce the root-mean-square current. In [152], a discrete extended phase-shift (DEPS) control scheme was proposed to improve the dynamic response of DAB DC-DC converters. The proposed DEPS control adjusts the transmission power of the DAB DC-DC converter by generating high- and low-power control pulses, which are preset to have discrete phase-shift ratios rather than pulse-width modulation control. In [153], a double-integral sliding-mode control and variable phase-shift algorithm were proposed. The control block diagram is shown in Figure 19. The dual-bridge DC/DC converter is operated in a phase-shifting operation to transfer the desired power to either V2G or G2V mode. During the G2V mode of operation, the primary side of the DAB converter operates with a leading phase-shift variation, whereas in V2G mode, the secondary side operates with leading-phase operation. The selector switch in the DAB controller receives a high or low logic signal to determine whether to use leading or lagging-edge phase-shift control to operate in G2V and V2G modes, respectively.

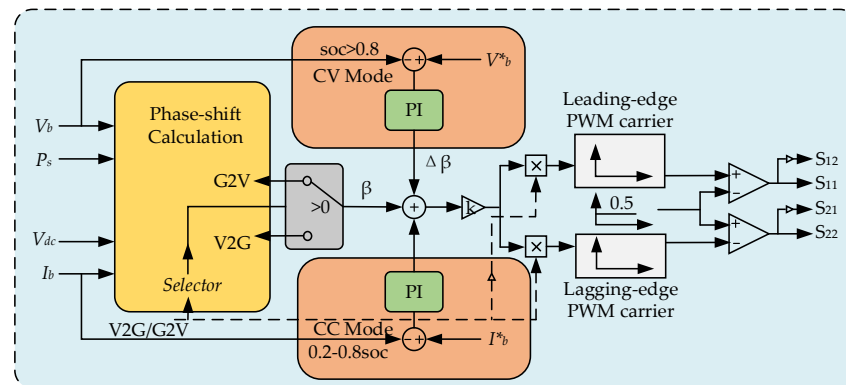


Figure 19. DAB phase shift algorithm.

The control method of the PSFB converter is similar to that of the DAB converter. SPS modulation is the most commonly used method to control the PSFB converter. The output power and voltage can be adjusted by changing the phase-shift angle, but it is difficult to achieve soft switching under light-load conditions. In [154], a new hybrid-mode control technology for the PSFB converter was proposed to improve efficiency under light- and heavy-load conditions. The control idea is to reduce the transformer turn ratio to reduce the circulating current, thereby reducing the circulating loss. In [113,155], an asymmetric pulse-width modulation strategy was adopted for the circulation problem so that the converter could achieve high efficiency in a wide range of output voltages. In [156], a new adaptive-burst-mode control strategy was proposed, which achieved a smaller effective switching frequency and lower switching loss. In [111], aiming to address some of the technical defects of PSFB converters in EV applications, such as the large circulating current and large reverse power, an improved control scheme was proposed by adjusting the phase-shift angle and duty cycle to increase the pre-charging stage and common charging stage. In the pre-charging stage, the voltage overshoot was suppressed. In the co-charging stage, the circulating current and the root-mean-square current of the transformer were effectively reduced. The long pre-charging time is the main reason for the reverse power and circulating current. This control method optimizes the pre-charging time and the control block diagram of the reverse operation is shown in Figure 20. The compensator is a PI controller, where k_p is the proportional gain and k_i is the integral gain. If the reference current is higher than I_{L0} , the co-charging time as $\varphi_1 T_s$ needs to be increased and vice versa. By sampling the input voltage V_{in} , output voltage V_o , and average input current I_{L0} , single-direction mode (SDM) and alternating-direction mode (ADM) can be judged using mode-selection calculations. In the sensing and diagnostic module of SDM, the pre-charge time can be calculated. In ADM, the pre-charge time is zero. Then, the driving signal can be obtained using φ_1 and T_{pre} . The model predictive control method has certain advantages in the case of multiple objectives and multiple physical constraints. In [157], a model predictive control method was proposed, which can effectively improve the dynamic characteristics of the center-tap PSFB converter. This method has the characteristics of fast dynamics and is robust to sudden changes in load impedance. In [158], an efficient model predictive control algorithm based on the Laguerre function was proposed for the PSFB converter. This method uses the system dynamics model to transform the nonlinear peak inductor current constraint into a dynamic linear constraint.

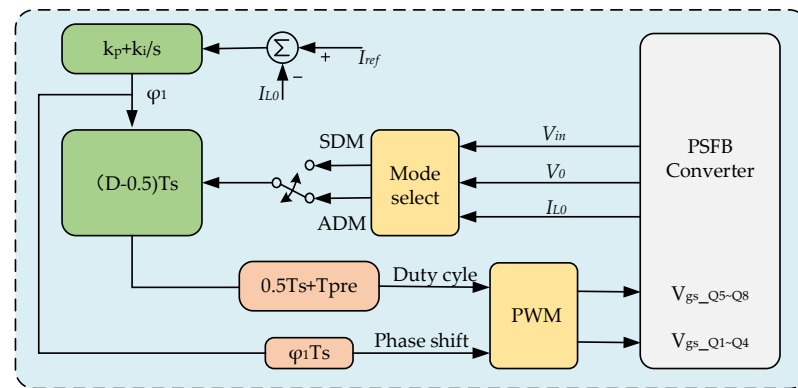


Figure 20. Simplified control chart of PSFB reverse operation.

This section discusses various DC/DC converter control methods suitable for fast-charging systems. Some general control methods can be applied to a variety of topologies, such as pulse-width modulation control, frequency modulation control, double closed-loop PI control, phase-shift control, and double phase-shift control, among others, which are suitable for the LLC resonant converter, DAB converter, PSFB converter, and other topologies. Model predictive control, sliding-mode control, and burst-mode control are also applicable to a variety of topologies.

8. Impact of High-Power Fast Charging on Power Batteries

The power battery is the key component of electric vehicles and is the premise and foundation of the stable operation of EVs. Electric vehicles with high-power charging have some impact on the battery body [159], such as low charging efficiency, reduced battery cycle charging times, battery aging, and reduced battery capacity. It may also cause battery thermal runaway and can even affect safety.

8.1. Factors Influencing Fast Charging of Power Batteries

The lithium battery is affected by the state of charge, temperature, and charging current of the battery during the fast-charging process and these factors have strong coupling [160]. The influencing factors of the fast charging of power batteries are shown in Figure 21.

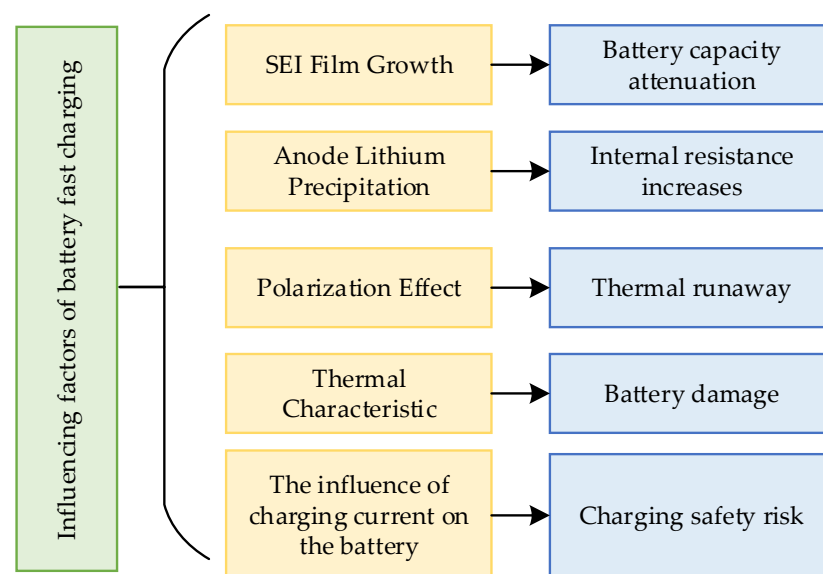


Figure 21. Factors influencing fast charging of power batteries.

1. SEI Film Growth.

When a lithium battery is charged and discharged for the first time, the anode reacts electrochemically with the electrolyte and an SEI film is formed at the anode interface [161]. The formation of the SEI film causes the irreversible loss of the partial capacity of the lithium battery and increases the internal resistance of the battery. In [162], the effect of the charging-current rate on the aging of ternary lithium batteries was analyzed. It was found that a high charging-current rate increased the growth rate of SEI film, which further led to the increase in battery impedance and aggravated capacity attenuation.

2. Anode Lithium Precipitation.

Lithium precipitation on the anode causes the battery capacity to decay. The precipitated lithium metal is typically attached to the surface of the negative electrode particles in the form of lithium dendrites. After a certain amount of growth, the lithium dendrites can pierce the diaphragm, causing the positive and negative electrodes to short circuit, which, in turn, causes thermal runaway. In [163], the lithium evolution potential was used to calibrate the lithium evolution current boundary of the lithium battery. In other words, based on the negative potential threshold, the negative lithium evolution side-reaction boundary current of the lithium battery during the fast-charging process was used as the maximum charging current for the entire battery charging range.

3. Polarization Effect.

The polarization of lithium batteries is affected by factors such as the charge and discharge current, ambient temperature, internal active material concentration, etc. The polarization phenomenon hinders the dynamic characteristics of lithium ions, resulting in an increase in temperature, anode lithium precipitation, etc., making the charging-current curve unable to track the maximum charging-current curve. When the polarization is serious, it can cause the battery voltage to rise sharply and damage the battery [164]. In [165], the pulse-duty cycle was adjusted by reducing the concentrated polarization to ensure that distributed batteries can be safely charged in the temperature range of 5 °C to 45 °C. The proposed charging process completed about 80% of its maximum capacity in less than 20 min without damaging the battery characteristics.

4. Thermal Characteristics.

Lithium batteries generate heat during fast charging, mainly manifested as chemical heat, polarization heat, ohmic heat, and side-reaction heat. Since the capacity of a certain type of lithium battery does not change much during use, the chemical heat of the battery also does not change much, whereas the polarization heat, ohmic heat, and side-reaction heat are all related to the charging strategy adopted by the battery. The higher the polarization degree of the battery, the more severe the side reaction and the more heat generated, which accelerates the rate of the temperature increase of the battery [166]. In [167], two lithium-ion batteries were compared and the thermal images during the profiling process were recorded to observe the temperature distribution. At the same time, three ambient temperatures were tested. The analysis showed that when the temperature was lower than 35 °C, fast charging could be applied to lithium batteries. When the temperature exceeded the safe boundary temperature, it caused a thermal runaway if not controlled.

5. The influence of the charging current on the battery.

The charging-current rate can affect the life cycle of lithium batteries, and the battery capacity curve at different charging-current rates first shows a decrease and then an increase [168]. When the number of battery cycles exceeds 300, the maximum available capacity of the battery decreases sharply under the condition of high-rate current charging. Increasing the upper charge voltage can suppress the battery capacity decay. This is because increasing the upper charge voltage increases the potential difference between the positive and negative electrodes, which leads to more lithium ions being embedded into the negative electrode. However, when the charging voltage is too high, the negative potential drops

below 0 V, which leads to the evolution of the anode lithium, resulting in a sharp decline in battery capacity. Under the condition of fast charging, the negative electrode potential and current density should be monitored to avoid lithium precipitation and reduce the risks to charging safety. In [169], the first-order equivalent circuit model of the battery was used to analyze the variables affecting the charging process, and the influence of the current rate on the internal resistance was discussed. Through experiments, it was concluded that a high-rate charging current has a significant effect on the fast-charging performance of the battery. Charging the battery at 6C can significantly improve the charging speed.

8.2. Fast-Charging Method of Power Batteries

To effectively reduce the impact of fast charging on the power battery of an EV, a variety of charging methods have been derived. The following are some of the mainstream charging methods [170,171].

1. Pulse Charging.

Compared with conventional charging methods, pulse charging can charge at a larger current and the concentration polarization and ohmic polarization of the battery are eliminated during the shutdown period so that the next round of charging is carried out more smoothly. The charging speed is fast, the temperature change is small, and the battery life is small so this method is widely used. Compared to traditional CC charging, a short break is added during the charging process, which gives the lithium battery a stronger charging acceptance ability. At the same time, it can eliminate the polarization voltage, inhibit the growth of lithium dendrites, slow down the aging of the battery, and accelerate the charging speed [172]. In [173], the effects of low-frequency positive pulse-current (PPC) charging on the life and charging performance of lithium-ion batteries were studied experimentally. It was found that compared to traditional CC charging, the life, maximum temperature, and energy efficiency of lithium-ion batteries using the PPC charging cycle increased by 81.6%, 60.5%, and 9.1%, respectively, after 1000 cycles.

2. Multi-stage constant-current charging.

Multi-stage constant-current charging refers to dividing the charging current into multiple segments according to certain rules. Each current is a fixed constant. After charging to a set threshold with a specific constant current, it continues to charge with another constant current until the battery capacity reaches the set value. In [174], an orthogonal experimental scheme for multi-objective coordinated multi-stage current optimization was designed and a five-stage constant current (5SCC) optimization strategy was proposed based on two orthogonal experiments. Compared to the traditional CC-CV charging strategy, the 5SCC charging strategy has good application prospects in terms of charging time and charging power. In [175], a variable-inductance binary operation method was proposed to realize different constant-current stages, and the voltage-controlled semi-active rectifier was controlled to ensure the efficient operation of the converter.

3. Positive and negative pulse charging.

The working cycle of positive and negative pulse charging involves three stages: positive charging, reverse instantaneous discharge, and stop charging. It solves the polarization phenomenon of the battery to a large extent and accelerates the charging speed but reverse discharge can shorten the life of the lithium battery. In [176], a method of using a supercapacitor to absorb and store high-energy negative pulses in the charging process of positive and negative pulses was proposed. When the amount of electricity stored in the supercapacitor reached the set value, this part of the electricity was used to charge the lithium-ion battery CV. Compared with the traditional positive and negative pulse methods, the energy utilization rate increased by 19%.

4. Optimal fast-charging strategy.

The main research objectives of the lithium battery charging strategy comprise four aspects: minimizing charging time, maximizing efficiency, maximizing capacity, and maxi-

mizing the life cycle. However, there is a competitive relationship between these targets. Shortening the charging time requires increasing the current rate and the high-rate current also increases the polarization voltage, thereby reducing the charging efficiency. Therefore, it is necessary to balance the relationship between the different objectives based on the battery characteristics to achieve rapid charging. In [177], a new multi-stage constant-heating-rate optimization method based on a genetic algorithm (offline strategy) was proposed, which effectively reduced the charging time and the increase in temperature. The results showed that at ambient temperatures, 10 °C, 25 °C, and 40 °C, compared to the average charging time of the CC-CV method, the charging time of the proposed method was shortened by 1.9%, 5.3%, 8.56%, and 9.54%, respectively, and the increase in temperature was reduced by 48.6%, 28.3%, 67.3%, and 17.9%, respectively. In [178], an optimal charging strategy with constant power injection was proposed. Based on the electric vehicle charging billing system, the charging strategy provides an optimal charging power reference to minimize the cost of the charging energy, charging time, and available energy loss. The results showed that the proposed charging strategy can minimize the loss of battery capacity and the economic burden on users.

To meet the demand for increased charging speeds, many automobile manufacturers have invested a lot of time in investigating and implementing fast-charging strategies, but there are still many deficiencies [179]. The main challenges in the safe and fast charging of lithium batteries are as follows. First, the battery itself can withstand a large charging current, which has higher requirements for the battery polarization resistance. Second, the battery can maintain good working performance, life cycle, and thermal safety after being charged at a high-rate current, which requires the active material of the battery to be reliable in terms of stability.

8.3. The Influence of the Battery Management System on Power Batteries

Research into battery management systems (BMS) is necessary for the fast charging of electric vehicles [180]. There are two main functions of BMS: they provide stable and reliable energy for new-energy electric vehicles and they improve the service time and life of power batteries through the charge and discharge balance of the batteries. The battery management system is integrated into the power battery. The quality of the battery management decision directly affects the battery life and the stability and safety of the vehicle. The working characteristics and life of the battery are significantly influenced by the temperature. The main functions of battery thermal management involve rapidly heating the battery pack when ambient temperatures are too low to ensure the battery is operating in an optimal condition; achieving effective heat dissipation and ventilation of the battery pack when ambient temperatures are too high; and identifying the temperature field range while ensuring uniform temperature distribution [181,182]. In [183], the current research priorities were summarized and some possible new research directions were proposed for more efficient thermal management systems. Three important types of thermal management strategies were discussed: air management, fluid management, and phase-change materials.

One of the important functions of BMS is the accurate prediction and monitoring of the state of charge (SOC) of each battery in the battery pack, which is essential for the safety and charge balance of electric vehicles [184]. In [185], a data-driven method was used to propose a transfer learning framework by considering adaptive conditional probability distribution, which addressed the influence of battery pack differences, temperature, aging, and other factors on SOC prediction. In [186], the authors proposed an effective health status indicator and remaining useful life prediction method for lithium-ion batteries based on a moving window approach to predict the remaining useful life of the battery. The experimental data tested at different current rates (including 1 °C and 2 °C) and different temperatures (including 25 °C and 40 °C) were collected and used. The implementation results showed that the capacity estimation error was within 1.5%.

9. Development Trends

9.1. Trends in Charging Infrastructure

With the large-scale promotion of electric vehicles, the construction and deployment of charging facilities have become the main reason restricting the development of the electric vehicle industry [187]. In the early stages of electric vehicle development, class I and class II slow charging were the most widely used charging methods. The slow-charging method is suitable for private cars, unit group cars, and other vehicles with a short travel time and long-term idle state. These vehicles can be charged for a long time during the low electricity trough at night, which has less of an impact on the power grid and provides power grid support, such as load balancing, frequency, and voltage regulation [188]. Slow-charging facilities typically involve AC charging piles, which are used to charge electric vehicles through on-board charging machines, as they provide small power but a full charging speed. The cost of a single AC slow-charging pile is about USD 300–900, and its construction cost composition is shown in Figure 22. Generally speaking, the cost of AC charging piles is low, economical, and affordable, and is mostly used in residential charging piles.

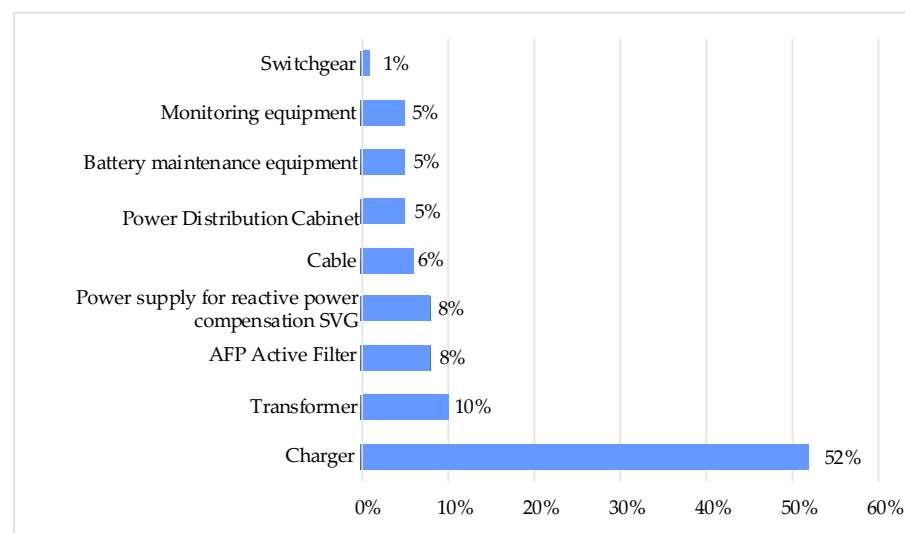


Figure 22. Construction cost analysis diagram of slow-charging piles.

With the gradual spread of electric vehicles, slow charging can no longer meet the daily needs of users. Fast charging is mainly used for private cars, taxis, and other vehicles that require emergency charging because the remaining power of the vehicles cannot meet users' travel needs [189,190]. Fast charging not only reduces the charging time but also provides the convenience of using the same charging interface for all electric vehicles, making it easier to promote and user-friendly. However, fast-charging equipment has high costs, a large volume, and requires ancillary equipment and a large land area. The construction input of a single 100 kW DC charging pile is shown in Table 4. The cost of the equipment (including the cost of the monitoring system) is about 0.07 USD/W and the cost of the 100 kW DC charging pile is about USD 7300. The cost of civil construction is about USD 2700–3800 and the cost of the power distribution side equipment is about USD 6400. Generally speaking, DC charging piles have high costs and fast charging speeds and are typically used in public parking lots, highway service areas, and other places.

Table 4. Cost analysis of 100 kW DC charging pile.

Investment Section	Specific Content	Cost (USD)
Charging facilities (including monitoring)	Charging module, box, relay, electricity metering system, etc.	7300
Distribution side	Box transformers, low-voltage electrical appliances, electric meters, etc.	6400
Civil construction and materials	Building construction, wires, cables, etc.	2700–3800

With advancements in technology, the ability to assemble quick-filling piles has become possible [191]. In the future, the construction of charging facilities should be based on unified standards and policies issued by the state, the charging interface should be unified, the charging mode should be clear, and the charging facilities should be universal so that the charging needs of different users can be met. In addition, based on existing road traffic, as well as the building layout of the city, the site selection of charging stations should be carried out in combination with city and power grid planning authorities to ensure the safety of personnel and convenient charging for users. Inductive roadbed charging systems are also a future development trend, as they can continuously charge electric vehicles in designated charging lanes on roads, thereby increasing the driving range of electric vehicles and reducing the battery size [192].

9.2. Future Trends in Electric Vehicles

In recent years, the electric vehicle industry has grown rapidly and fast-charging systems that can charge electric vehicle batteries to more than 80% in 20 min are the focus of research in this field [193]. Figure 23 shows the strategic planning of charging systems of some well-known car companies. Mercedes-Benz is expected to launch a 50 kW 800 V fast-charging model after 2023, which can be charged to 80% in 15–20 min. Audi is expected to launch the A6 e-tron concept model in 2024, which will be the first pure electric limousine based on the PPE platform. The power battery capacity is 100 kWh and the NEDC mileage is 700 km. It can increase the driving range by 300 km with just 10 min of charging and the SOC can be increased from 5% to 80% in just 25 min of charging [194]. Tesla updated the Supercharger V3 network in 2021 and the maximum output power has increased from 250 kW to 300 kW. Tesla will launch an 800 V platform and models based on this platform should be released with 46,800 batteries. The Volkswagen MEB platform has a typical fast-charging capability, which can achieve a 40 min SOC increase from 30% to 80%. The company's next development focus is the scalable system platform, which is expected to serve as the foundation for the launch of electric vehicles in 2025 [195]. Hyundai and Kia jointly launched the E-GMP platform, which supports 800 V fast charging. In the next few years, models based on this platform are expected to be mass-produced [196]. NIO has upgraded its third-generation digital platform NT 3.0, including the electronic and electrical architecture, electronic control, an intelligent cockpit, and intelligent driving technology. It is expected to launch related models in 2024 [197]. Li Auto Inc. launched two platforms: a space-oriented Whale platform and a performance-oriented Shark platform. The fast-charging performance of the first electric vehicle is 800 V–400 kW and the SOC increases from 10% to 80% in 10–15 min. It is expected to be mass-produced in 2023 [198]. BYD has launched the e-platform 3.0, which is based on the 800 V platform and can support a charging power of 228 kW or higher, resulting in a 150 km increase in cruising range after just 5 min of charging. The platform's representative models have already entered mass production, and BYD plans to launch more models in the future [199]. LEAPMOTOR announced its 800 V ultra-high-voltage electrical platform in 2021, which can support up to 400 V charging and achieve a cruising range of 200 km and above in just 5 min of charging. The corresponding models will be mass-produced in the fourth quarter of 2024. In 2021, China Chang'an Automobile Group (CCAG, Chongqing, China) released an 800 V electric drive platform. The new generation of electric vehicle platform models can increase the cruising range by 200 km in just 10 min of charging. According to its plans, the company

will launch two series of products in the future: 450 V and 800 V, covering a voltage range of 240 V–800 V, to meet power demands ranging from 160 to 300 kW, with a maximum mileage range of 400–1000 km [200].

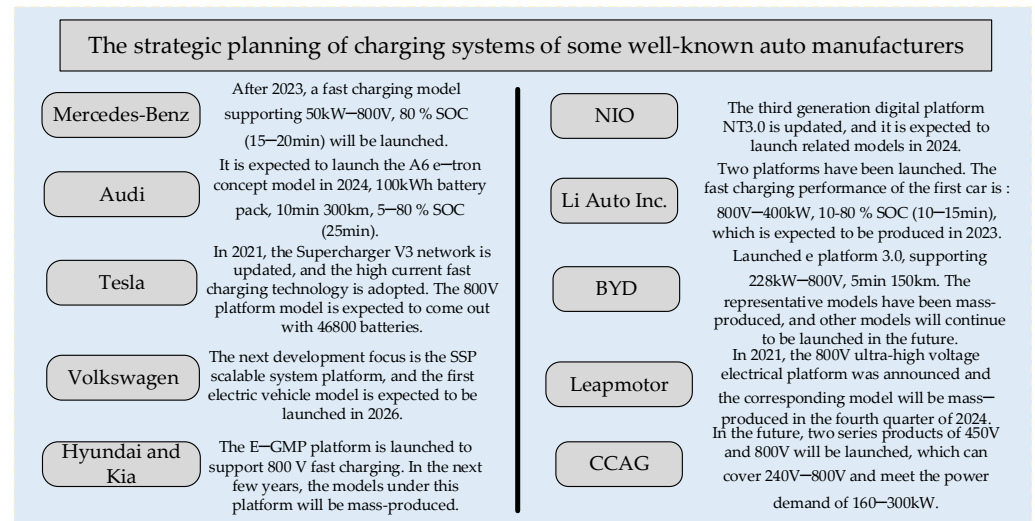


Figure 23. Strategic planning of the charging systems of some well-known car companies.

It can be seen from the strategic planning of the above car companies that high-power fast-charging technology is an inevitable trend for the future development of EVs. However, overcoming the challenges of fast charging requires detailed research on charging cables, cooling methods, protection devices, efficient power converter design, battery materials, and energy storage. As they are an important component of EVs, the market demand for power batteries is also expanding rapidly. In terms of batteries, improvements in storage capacity, battery materials, and manufacturing processes are future development directions [201]. Energy storage can be equipped with supercapacitors, which offer benefits such as high power density, long life cycle, wide temperature range, and require minimal maintenance. Batteries can be made of graphene, which has good electrical conductivity and is lightweight, strong, and tough. In terms of charging efficiency, graphene batteries have a significantly higher charging capacity than traditional batteries, their service life is twice that of lithium batteries and four times that of hydrogenated batteries, and their weight is only about 50% of traditional batteries. However, due to various reasons such as costs, the large-scale promotion of graphene batteries still faces some problems. The development of automobile power batteries is expected to focus on long cells and large modules. By using laminated technology, the energy density can be increased by 5%, the life cycle can be increased by 10%, and the costs can be reduced by 15%.

V2G aims to use EVs as both a travel tool and a mobile energy storage device [202]. V2G guides EVs to discharge when the power grid is insufficient and charge when the power grid is at its peak and uses incentives such as electricity prices to realize the interaction between EVs and the power grid. At the same time, EVs can be used as power sources to power other devices, including vehicle-to-vehicle, vehicle-to-infrastructure, vehicle-to-human, vehicle-to-external network, and other application scenarios [203]. V2G provides a more flexible and economical energy storage mode for the power grid and provides a new solution for grid connections and the economic dispatch of EVs [204].

10. Conclusions

To further reduce the charging time of EVs, high-power fast charging has become an important development direction for EV charging technology. This paper discusses the development status, system architecture, and related standards of electric vehicle fast-charging systems, the topology and control technology of power converters, the influence

of high-power fast charging on power batteries, and future development trends. The topologies of the front-stage AC/DC converter and the rear-stage DC/DC converter for the fast-charging system are comprehensively analyzed and the advantages and disadvantages of the related topologies are summarized. Additionally, the control strategies of the front-stage AC/DC converter and the rear-stage DC/DC converter are studied. The control target of the front-stage AC/DC converter is to output a stable voltage on the DC side and the AC side realizes the unit's power factor operation. The goal of the control target of the rear-stage DC/DC converter is to achieve ZVS in the full load range, reduce the current ripple, and improve system efficiency. The promotion of fast-charging technology for EVs depends largely on the efficiency, cost, safety, reliability, and control methods of the converter topology. The fast charging of EVs will also have an impact on power batteries. The optimization of charging methods and improvement of battery materials will become important factors in the widespread popularity of fast-charging technology. The application of V2G can effectively reduce the cost of EVs and could become the key to the popularization of electric vehicles.

Author Contributions: Conceptualization, K.Z. and X.W.; Methodology, K.Z., Y.W. and Y.S.; Software, Y.W., D.T. and Y.L.; Supervision, K.Z. and X.W.; Writing—review and editing, Y.W., Y.S., D.T. and Y.L. All authors have read and agreed to the published version of the manuscript.

Funding: This research was funded by The Open Fund Project of the State Key Laboratory of Automotive Safety and Energy, grant number KFY2222.

Data Availability Statement: Not applicable.

Conflicts of Interest: The authors declare no conflict of interest. The funders had no role in the design of the study; in the collection, analyses, or interpretation of data; in the writing of the manuscript; or in the decision to publish the results.

References

1. Yu, D.M.; Yang, C.; Jiang, L.R.; Li, T.Y.; Yan, G.G.; Gao, F.K.; Liu, H.N. Review on Safety Protection of Electric Vehicle Charging. *Proc. Chin. Soc. Elect. Eng.* **2022**, *42*, 2145–2164.
2. James, D.; Keith, B. Electric vehicles, Battery Capacity, Charger Power, Access to Charging and the Impacts on Distribution Networks. *eTransportation* **2020**, *4*, 100059.
3. IEA. Global EV Outlook 2022. IEA: Paris, France, 23 May 2022. Available online: <https://www.iea.org/reports/global-ev-outlook-2022> (accessed on 12 January 2023).
4. IEA. Global Electric Car Stock, 2010–2021. IEA: Paris, France, 23 May 2022. Available online: <https://www.iea.org/data-and-statistics/charts/global-electric-car-stock-2010-2021> (accessed on 12 January 2023).
5. Tong, M.H.; Cheng, M.; Xu, Z.H.; Wen, H.H.; Hua, W.; Zhu, X.Y. Key Issues and Solutions of Integrated On-Board Chargers for Electric Vehicles. *Trans. China Electrotech. Soc.* **2021**, *36*, 5125–5142.
6. Khan, I.; Iqbal, A.; Sanjeevikumar, P.; Mitolo, M.; Shahidehpour, M.; Gueerero, J.M.; Holm-Nielsen, J.B.; Lam, J.; Marzband, M. Guest Editorial: Fast, Superfast, and Ultra-Superfast Intelligent and Smart Charging Solutions for Electric Vehicles. *IEEE Trans. Ind. Appl.* **2022**, *58*, 5518–5519. [[CrossRef](#)]
7. Vasiladiotis, M.; Rufer, A. A Modular Multiport Power Electronic Transformer with Integrated Split Battery Energy Storage for Versatile Ultrafast EV Charging Stations. *IEEE Trans. Ind. Electron.* **2015**, *62*, 3213–3222. [[CrossRef](#)]
8. IEA. Fast Publicly Available Chargers, 2015–2021. IEA: Paris, France, 23 May 2022. Available online: <https://www.iea.org/data-and-statistics/charts/fast-publicly-available-chargers-2015-2021> (accessed on 12 January 2023).
9. IEA. Slow Publicly Available Chargers, 2015–2021. IEA: Paris, France, 23 May 2022. Available online: <https://www.iea.org/data-and-statistics/charts/slow-publicly-available-chargers-2015-2021> (accessed on 12 January 2023).
10. Rizwan, K.M.; Saad, A.M.; Adil, S.; Asghar, J. A Comprehensive Review on Electric Vehicles Charging Infrastructures and Their Impacts on Power-Quality of the Utility Grid. *eTransportation* **2019**, *1*, 100006.
11. Tao, Y.C.; Qiu, J.; Lai, S.Y.; Sun, X.Z.; Zhao, J.H. Adaptive Integrated Planning of Electricity Networks and Fast Charging Stations Under Electric Vehicle Diffusion. *IEEE Trans. Power Syst.* **2023**, *38*, 499–513. [[CrossRef](#)]
12. Tim, U.; Jeppe, R.; Bach, A.P.; Seyedmostafa, H. Electric Vehicle Charging Infrastructure Planning for Integrated Transportation and Power Distribution Networks: A Review. *eTransportation* **2022**, *12*, 100163.
13. Ding, M.; Shi, S.L.; Pan, H.; Wang, M.; Yao, Y.L. Planning of AC/DC Hybrid Microgrid with Integration of Electric Vehicles Charging Load. *Autom. Electr. Power Syst.* **2018**, *42*, 32–38+81.
14. Jahnes, M.; Zhou, L.; Eull, M.; Wang, W.Z.; Preindl, M. Design of a 22-kW Transformerless EV Charger with V2G Capabilities and Peak 99.5% Efficiency. *IEEE Trans. Ind. Electron.* **2023**, *70*, 5862–5871. [[CrossRef](#)]

15. Jan, E.; Martin, Z.J.; Tatiana, G.; Mattia, M. Energy Management of a Multi-Battery System for Renewable-Based High Power EV Charging. *eTransportation* **2022**, *14*, 100198.
16. Trivedi, N.; Gujar, N.S.; Sarkar, S.; Pundir, S.P.S. Different Fast Charging Methods and Topologies for EV Charging. In Proceedings of the 2018 IEEMA Engineer Infinite Conference (eTechNxT), New Delhi, India, 13–14 March 2018; pp. 1–5.
17. Franzese, P.; Pasquale, A.D.; Iannuzzi, D.; Pagano, M. Electric Ultra Fast Charging Stations: A Real Case Study. In Proceedings of the 2021 AEIT International Annual Conference (AEIT), Milan, Italy, 4–8 October 2021; pp. 1–6.
18. Li, Q.F.; Shi, Y.; Kang, J.Y.; Feng, L.L. A novel high-power ZVZCS three-level DC-DC converter is presented. *J. Power Supply* **2022**, *20*, 34–44.
19. Vuchev, S.A. Analytical Investigation of Converter for Electric Vehicle Fast Charging. In Proceedings of the 2018 IX National Conference with International Participation (ELECTRONICA), Sofia, Bulgaria, 17–18 May 2018; pp. 1–4.
20. Mishra, S.; Sahu, L.K.; Tiwari, A.K.; Chander, A.H. Modelling of Electric Vehicle Direct Current Fast Charging Station. In Proceedings of the 2021 Asian Conference on Innovation in Technology (ASIANCON), PUNE, India, 27–29 August 2021; pp. 1–5.
21. Anzola, J.; Aizpuru, I.; Arruti, A. Non-Isolated Partial Power Converter for Electric Vehicle Fast Charging Stations. In Proceedings of the 2020 IEEE 11th International Symposium on Power Electronics for Distributed Generation Systems (PEDG), Dubrovnik, Croatia, 28 September–1 October 2020; pp. 18–22.
22. Camurca, L.; Pereira, T.; Hoffmann, F.; Liserre, M. Analysis, Limitations, and Opportunities of Modular Multilevel Converter-Based Architectures in Fast Charging Stations Infrastructures. *IEEE Trans. Power Electron.* **2022**, *37*, 10747–10760. [[CrossRef](#)]
23. Zheng, L.; Kandula, R.P.; Divan, D. Multiport Control With Partial Power Processing in Solid-State Transformer for PV, Storage, and Fast-Charging Electric Vehicle Integration. *IEEE Trans. Power Electron.* **2023**, *38*, 2606–2616. [[CrossRef](#)]
24. Ahmad, A.; Qin, Z.; Wijekoon, T.; Bauer, P. An Overview on Medium Voltage Grid Integration of Ultra-Fast Charging Stations: Current Status and Future Trends. *IEEE Open J. Ind. Electron. Soc.* **2022**, *3*, 420–447. [[CrossRef](#)]
25. Li, C.B.; Mi, G.X.; Li, X.; Liu, W.Q. An High-power Electric Vehicle Quick Charger. *Power Electron.* **2016**, *50*, 99–101.
26. Gao, X.; Carne, G.D.; Andresen, M.; Bruske, S.; Pugliese, S.; Liserre, M. Voltage-Dependent Load-Leveling Approach by Means of Electric Vehicle Fast Charging Stations. *IEEE Trans. Transp. Electr.* **2021**, *7*, 1099–1111. [[CrossRef](#)]
27. Kabir, M.E.; Assi, C.; Alameddine, H.; Antoun, J.; Yan, J. Demand-Aware Provisioning of Electric Vehicles Fast Charging Infrastructure. *IEEE Trans. Veh. Technol.* **2020**, *69*, 6952–6963. [[CrossRef](#)]
28. SAE International. *Electric Vehicle and Plug in Hybrid Electric Vehicle Conductive Charge Coupler*; SAE International: Warrendale, PA, USA, 2017.
29. Srdic, S.; Lukic, S. Toward Extreme Fast Charging: Challenges and Opportunities in Directly Connecting to Medium-Voltage Line. *IEEE Electr. Mag.* **2019**, *7*, 22–31. [[CrossRef](#)]
30. Purgat, P.; van der Blij, N.H.; Qin, Z.; Bauer, P. Partially Rated Power Flow Control Converter Modeling for Low-Voltage DC Grids. *IEEE J. Emerg. Sel. Top. Power Electron.* **2020**, *8*, 2430–2444. [[CrossRef](#)]
31. Sharma, G.; Sood, V.K.; Alam, M.S.; Shariff, S.M. Comparison of Common DC and AC Bus Architectures for EV Fast Charging Stations and Impact on Power Quality. *eTransportation* **2020**, *5*, 100066. [[CrossRef](#)]
32. Ronanki, D.; Kelkar, A.; Williamson, S.S. Extreme Fast Charging Technology-Prospects to Enhance Sustainable Electric Transportation. *Energies* **2019**, *12*, 3721. [[CrossRef](#)]
33. Safayatullah, M.; Elraisi, M.T.; Ghosh, S.; Rezaei, Z.; Batarseh, I. A Comprehensive Review of Power Converter Topologies and Control Methods for Electric Vehicle Fast Charging Applications. *IEEE Access* **2022**, *10*, 40753–40793. [[CrossRef](#)]
34. Yilmaz, M.; Krein, P.T. Review of Battery Charger Topologies, Charging Power Levels, and Infrastructure for Plug-In Electric and Hybrid Vehicles. *IEEE Trans. Power Electron.* **2013**, *28*, 2151–2169. [[CrossRef](#)]
35. *IEEE Application Guide for IEEE Std 1547TM*; IEEE Standard for Interconnecting Distributed Resources with Electric Power Systems. IEEE: New York, NY, USA, 2009.
36. Zhen, Z.J.; Meng, X.F. State of the Art and Research of the Charging Coupler Standards in China and Aboard. *Chin. J. Automot. Eng.* **2012**, *2*, 1–7.
37. International Electrotechnical Commission. *Plugs, Socket-Outlets, Vehicle Connectors and Vehicle Inlets-Conductive Charging of Electric Vehicles-Part 3: Dimensional Compatibility and Interchangeability Requirements for d.c. and a.c./d.c. Pin and Contact-Tube Vehicle Couplers: IEC 62196-3:2014*; IEC: Geneva, Switzerland, 2014.
38. SAE International. *Combined Charging System 1.0 Specification-CCS 1.0*. CCS 1.0; SAE International: Warrendale, PA, USA, 2012.
39. CHAdeMO Association. *Technical Specifications of Quick Charger for the Electric Vehicle: CHAdeMO 1.0.0*; CHAdeMO Association: Tokyo, Japan, 2012.
40. National Technical Committee of Auto Standardization. *Connection Set for Conductive Charging of Electric Vehicles-Part 3: DC Charging Coupler: GB/T 20234.3-2015*; Standards Press of China: Beijing, China, 2016.
41. Khaligh, A.; D’Antonio, M. Global Trends in High-Power On-Board Chargers for Electric Vehicles. *IEEE Trans. Veh. Technol.* **2019**, *68*, 3306–3332. [[CrossRef](#)]
42. CHAdeMO Association. *Technical Paper of High-Power Charger for Electric Vehicles for CHAdeMO 3.0/Chaoji Type 2*; CHAdeMO Association: Tokyo, Japan, 2020.
43. Yong, J.Y.; Ramchandaramurthy, V.K.; Miao, T.K.; Selvaraj, J. Experimental Validation of a Three-Phase Off-Board Electric Vehicle Charger with New Power Grid Voltage Control. *IEEE Trans. Smart Grid* **2018**, *9*, 2703–2713. [[CrossRef](#)]

44. Kesler, M.; Kisacikoglu, M.C.; Tolbert, L.M. Vehicle-to-Grid Reactive Power Operation Using Plug-In Electric Vehicle Bidirectional Offboard Charger. *IEEE Trans. Ind. Electron.* **2014**, *61*, 6778–6784. [[CrossRef](#)]
45. Yildirim, D.; Ozturk, S.; Cadirci, I.; Ermis, M. All SiC PWM Rectifier-based Off-board Ultrafast Charger for Heavy Electric Vehicles. *IET Power Electron.* **2020**, *13*, 483–494. [[CrossRef](#)]
46. Monteiro, V.; Ferreira, J.C.; Nogueiras, M.A.A.; Couto, C.; Afonso, J.L. Experimental Validation of a Novel Architecture Based on a Dual-Stage Converter for Off-Board Fast Battery Chargers of Electric Vehicles. *IEEE Trans. Veh. Technol.* **2018**, *67*, 1000–1011. [[CrossRef](#)]
47. Ma, Z.Y.; Xu, D.H.; Li, R.; Du, C.R.; Zhang, X. A Novel DC-Side Zero-Voltage Switching (ZVS) Three-Phase Boost PWM Rectifier Controlled by an Improved SVM Method. *IEEE Trans. Power Electron.* **2012**, *27*, 4391–4408. [[CrossRef](#)]
48. Kolar, J.W.; Friedli, T. The Essence of Three-Phase PFC Rectifier Systems—Part I. *IEEE Trans. Power Electron.* **2013**, *28*, 176–198. [[CrossRef](#)]
49. Adhikari, J.; IV, P.; Panda, S.K. Reduction of Input Current Harmonic Distortions and Balancing of Output Voltages of the Vienna Rectifier Under Supply Voltage Disturbances. *IEEE Trans. Power Electron.* **2017**, *32*, 5802–5812. [[CrossRef](#)]
50. Ding, W.L.; Zhang, C.H.; Gao, F.; Duan, B.; Qiu, H. A Zero-Sequence Component Injection Modulation Method with Compensation for Current Harmonic Mitigation of a Vienna Rectifier. *IEEE Trans. Power Electron.* **2019**, *34*, 801–814. [[CrossRef](#)]
51. Song, W.Z.; Xing, F.X.; Yan, H.; Empringham, L.; De Lillo, L.; Wheeler, P.; Li, J.; Zhong, Y.R. A Hybrid Control Method to Suppress the Three-Time Fundamental Frequency Neutral-Point Voltage Fluctuation in a VIENNA Rectifier. *IEEE J. Emerg. Sel. Top. Power Electron.* **2016**, *4*, 468–480. [[CrossRef](#)]
52. Rajendran, G.; Vaithilingam, C.A.; Naidu, K.; Oruganti, K.S.P. Energy-efficient Converters for Electric Vehicle Charging Stations. *SN Appl. Sci.* **2020**, *2*, 583. [[CrossRef](#)]
53. Cittanti, D.; Gregorio, M.; Bossotto, E.; Mandrile, F.; Bojoi, R. Full Digital Control and Multi-Loop Tuning of a Three-Level T-Type Rectifier for Electric Vehicle Ultra-Fast Battery Chargers. *Electronics* **2021**, *10*, 1453. [[CrossRef](#)]
54. Rajendran, G.; Vaithilingam, C.A.; Misron, N.; Naidu, K.; Ahmed, M.R. Voltage Oriented Controller Based Vienna Rectifier for Electric Vehicle Charging Stations. *IEEE Access* **2021**, *9*, 50798–50809. [[CrossRef](#)]
55. Ditze, S.; Ehrlich, S.; Weitz, N.; Sauer, M.; Aßmus, F.; Sacher, A.; Joffe, C.; Seßler, C.; Meißner, P. A High-Efficiency High-Power-Density SiC-Based Portable Charger for Electric Vehicles. *Electronics* **2022**, *11*, 1818. [[CrossRef](#)]
56. Zhao, S.S.; Borovic, U.; Silva, M.; Garcia, O.; Oliver, J.A.; Alou, P.; Cobos, J.A.; Pejovic, P. Modified VIENNA Rectifier III to Achieve ZVS in All Transitions: Analysis, Design, and Validation. *IEEE Trans. Power Electron.* **2021**, *36*, 13404–13422. [[CrossRef](#)]
57. Mallik, A.; Khaligh, A. Comparative Study of Three-phase Buck, Boost and Buck-boost Rectifier Topologies for Regulated Transformer Rectifier Units. In Proceedings of the 2015 IEEE Transportation Electrification Conference and Expo (ITEC), Dearborn, MI, USA, 14–17 June 2015; pp. 1–7.
58. Chen, Q.; Xu, J.P.; Tao, Z.Y.; Ma, H.B.; Chen, C. Analysis of Sector Update Delay and Its Effect on Digital Control Three-Phase Six-Switch Buck PFC Converters with Wide AC Input Frequency. *IEEE Trans. Power Electron.* **2021**, *36*, 931–946. [[CrossRef](#)]
59. Stupar, A.; Friedli, T.; Minibock, J.; Kolar, J.W. Towards a 99% Efficient Three-Phase Buck-Type PFC Rectifier for 400-V DC Distribution Systems. *IEEE Trans. Power Electron.* **2012**, *27*, 1732–1744. [[CrossRef](#)]
60. Ries, L.K.; Soeiro, T.B.; Ortmann, M.S.; Heldwein, M.L. Analysis of Carrier-Based PWM Patterns for a Three-Phase Five-Level Bidirectional Buck plus Boost-Type Rectifier. *IEEE Trans. Power Electron.* **2017**, *32*, 6005–6017. [[CrossRef](#)]
61. Wen, F.; Yuan, J.; Wickramasinghe, K.S.; Mayer, W.; Shabani, J.; Tutuc, E. Epitaxial Al-InAs Heterostructures as Platform for Josephson Junction Field-Effect Transistor Logic Devices. *IEEE Trans. Electron Devices* **2021**, *68*, 1524–1529. [[CrossRef](#)]
62. Guo, B.; Wang, F.; Aeloiza, E. A Novel Three-phase Current Source Rectifier with Delta-type Input Connection to Reduce the Device Conduction Loss. *IEEE Trans. Power Electron.* **2016**, *31*, 1074–1084. [[CrossRef](#)]
63. Lei, J.X.; Feng, S.; Zhao, J.F.; Chen, W.; Wheeler, P.; Shi, M.M. An Improved Three-Phase Buck Rectifier Topology with Reduced Voltage Stress on Transistors. *IEEE Trans. Power Electron.* **2020**, *35*, 2458–2466. [[CrossRef](#)]
64. Chen, Q.; Xu, J.P.; Zeng, F.; Huang, R.; Wang, L. An Improved Three-Phase Buck Rectifier with Low Voltage Stress on Switching Devices. *IEEE Trans. Power Electron.* **2021**, *36*, 6168–6174. [[CrossRef](#)]
65. Zhao, Y.F.; Yu, F.; Song, Q.G.; Zhu, Z.N.; Zhou, Y.C. A High Power Three-phase Buck Power Factor Correction Circuit with Low Switching Stress. *Proc. Chin. Soc. Elect. Eng.* **2021**, *41*, 318–325+421.
66. Soeiro, T.B.; Friedli, T.; Kolar, J.W. Design and Implementation of a Three-Phase Buck-Type Third Harmonic Current Injection PFC Rectifier SR. *IEEE Trans. Power Electron.* **2013**, *28*, 1608–1621. [[CrossRef](#)]
67. Friedli, T.; Hartmann, M.; Kolar, J.W. The Essence of Three-Phase PFC Rectifier Systems-Part II. *IEEE Trans. Power Electron.* **2014**, *29*, 543–560. [[CrossRef](#)]
68. Ahmed, M.A.; Dasika, J.D.; Saedifard, M.; Wasynczuk, O. Interleaved Swiss Rectifiers for Fast EV/PHEV Battery Chargers. In Proceedings of the 2014 IEEE Applied Power Electronics Conference and Exposition-APEC 2014, Fort Worth, TX, USA, 16–20 March 2014; pp. 3260–3265.
69. Olarescu, N.-V.; Ancuti, M.-C.; Sorandaru, C.; Musuroi, S.; Svoboda, M.; Hedes, A.; Popovici, D.; Wienmann, M. Performances/efficiency Analysis for High Efficiency Three-phase Buck-type PFC Rectifiers. In Proceedings of the 2015 17th European Conference on Power Electronics and Applications (EPE' 15 ECCE-Europe), Geneva, Switzerland, 8–10 September 2015; pp. 1–9.
70. Schrittwieser, L.; Leibl, M.; Haider, M.; Thony, F.; Kolar, J.W.; Soeiro, T.B. 99.3% Efficient Three-Phase Buck-Type All-SiC SWISS Rectifier for DC Distribution Systems. *IEEE Trans. Power Electron.* **2019**, *34*, 126–140. [[CrossRef](#)]

71. Zhang, B.F.; Xie, S.J.; Li, Z.Y.; Zhao, P.C.; Xu, J.M. An Optimized Single-Stage Isolated Swiss-Type AC/DC Converter Based on Single Full-Bridge with Midpoint-Clamper. *IEEE Trans. Power Electron.* **2021**, *36*, 11288–11297. [[CrossRef](#)]
72. Wong, C.S.; Liu, J.W.; Cao, L.L.; Loo, K.H. A SWISS-Rectifier-Based Single-Stage Three-Phase Bidirectional AC-DC Inductive-Power-Transfer Converter for Vehicle-to-Grid Applications. *IEEE Trans. Power Electron.* **2023**, *38*, 4152–4166. [[CrossRef](#)]
73. Abarzadeh, M.; Khan, W.A.; Weise, N.; Al-Haddad, K.; EL-Refaie, A.M. A New Configuration of Paralleled Modular ANPC Multilevel Converter Controlled by an Improved Modulation Method for 1 MHz, 1 MW EV Charger. *IEEE Trans. Ind. Appl.* **2021**, *57*, 3164–3178. [[CrossRef](#)]
74. Reis, F.E.U.; Torrico-Bascope, R.P.; Tofoli, F.L.; Bezerra, L.D. Bidirectional Three-Level Stacked Neutral-Point-Clamped Converter for Electric Vehicle Charging Stations. *IEEE Access* **2020**, *8*, 37565–37577. [[CrossRef](#)]
75. Tan, L.C.; Wu, B.; Venkata, Y.; Rivera, S.; Guo, X.Q. Effective Voltage Balance Control for Bipolar-DC-Bus-Fed EV Charging Station with Three-Level DC-DC Fast Charger. *IEEE Trans. Ind. Electron.* **2016**, *63*, 4031–4041. [[CrossRef](#)]
76. Rivera, S.; Wu, B.; Kouro, S.; Yaramasu, V.; Wang, J.C. Electric Vehicle Charging Station Using a Neutral Point Clamped Converter with Bipolar DC Bus. *IEEE Trans. Ind. Electron.* **2015**, *62*, 1999–2009. [[CrossRef](#)]
77. Choi, S.; Saeedifard, M. Capacitor Voltage Balancing of Flying Capacitor Multilevel Converters by Space Vector PWM. *IEEE Trans. Power Deliv.* **2012**, *27*, 1154–1161. [[CrossRef](#)]
78. Stillwell, A.; Candan, E.; Pilawa-Podgurski, R.C.N. Active Voltage Balancing in Flying Capacitor Multi-Level Converters with Valley Current Detection and Constant Effective Duty Cycle Control. *IEEE Trans. Power Electron.* **2019**, *34*, 11429–11441. [[CrossRef](#)]
79. Wen, F.; Shabani, J.; Tutuc, E. Josephson Junction Field-Effect Transistors for Boolean Logic Cryogenic Applications. *IEEE Trans. Electron Devices* **2019**, *12*, 5367–5374. [[CrossRef](#)]
80. Viatkin, A.; Ricco, M.; Mandrioli, R.; Kerekes, T.; Teodorescu, R.; Grandi, G. A Novel Modular Multilevel Converter Based on Interleaved Half-Bridge Submodules. *IEEE Trans. Ind. Electron.* **2023**, *70*, 125–136. [[CrossRef](#)]
81. Abronzini, U.; Attaianese, C.; Monaco, M.D.; Tomasso, G.; D’Arpino, M. Optimal Control for CHB Multi-Level Converter with Integrated ESS for EV Ultra-Fast Charging Station. In Proceedings of the 2018 IEEE International Conference on Electrical Systems for Aircraft, Railway, Ship Propulsion and Road Vehicles & International Transportation Electrification Conference (ESARS-ITEC), Nottingham, UK, 7–9 November 2018; pp. 1–6.
82. Zheng, T.; Wang, K.; Zheng, Z.D.; Pang, J.P.; Li, Y.D. Review of Power Electronic Transformers Based on Modular Multilevel Converters. *Proc. Chin. Soc. Elect. Eng.* **2022**, *42*, 5630–5649.
83. Heydari-doostabad, H.; O’Donnell, T. A Wide Range High Voltage Gain Bidirectional DC-DC Converter for V2G and G2V Hybrid EV Charger. *IEEE Trans. Ind. Electron.* **2022**, *69*, 4718–4729. [[CrossRef](#)]
84. Gupta, C.; Das, M. Multiphase Interleaved DC-DC Converter for Fast Charging Application of Electric Vehicles. In Proceedings of the 2022 IEEE 16th International Conference on Compatibility, Power Electronics, and Power Engineering (CPE-POWERENG), Birmingham, UK, 29 June–1 July 2022; pp. 1–6.
85. Kang, T.; Kim, C.; Suh, Y.; Park, H.; Kang, B.; Kim, D. A Design and Control of Bi-Directional Non-Isolated DC-DC Converter for Rapid Electric Vehicle Charging System. In Proceedings of the 2012 Twenty-Seventh Annual IEEE Applied Power Electronics Conference and Exposition (APEC), Orlando, FL, USA, 5–9 February 2012; pp. 14–21.
86. Alharbi, M.A.; Alcaide, A.M.; Dahidah, M.; P, M.R.; Ethni, S.; Pickert, V.; Leon, J.I. Rotating Phase Shedding for Interleaved DC-DC Converter-Based EVs Fast DC Chargers. *IEEE Trans. Power Electron.* **2023**, *38*, 1901–1909. [[CrossRef](#)]
87. Tan, L.C.; Wu, B.; Sebastian, R.; Yaramasy, V. Comprehensive DC Power Balance Management in High-Power Three-Level DC-DC Converter for Electric Vehicle Fast Charging. *IEEE Trans. Power Electron.* **2016**, *31*, 89–100. [[CrossRef](#)]
88. Tan, L.C.; Zhu, L.; Wu, B. An Integrated Inductor for Eliminating Circulating Current of Parallel Three-Level DC-DC Converter-Based EV Fast Charger. *IEEE Trans. Ind. Electron.* **2016**, *63*, 1362–1371. [[CrossRef](#)]
89. Zhou, L.W.; Jahnes, M.; Eull, M.; Wang, W.Z.; Preindl, M. Control Design of a 99% Efficiency Transformerless EV Charger Providing Standardized Grid Services. *IEEE Trans. Power Electron.* **2022**, *37*, 4022–4038. [[CrossRef](#)]
90. Yan, Z.X.; Zeng, J.; Lin, W.J.; Liu, J.F. A Novel Interleaved Nonisolated Bidirectional DC-DC Converter with High Voltage-Gain and Full-Range ZVS. *IEEE Trans. Power Electron.* **2020**, *35*, 7191–7203. [[CrossRef](#)]
91. Lee, B.K.; Kim, J.P.; Kim, S.G.; Lee, J.Y. A PWM SRT DC/DC Converter for 6.6-kW EV Onboard Charger. *IEEE Trans. Ind. Electron.* **2016**, *63*, 894–902. [[CrossRef](#)]
92. Ryu, S.H.; Kim, D.H.; Kim, M.J.; Kim, J.S.; Lee, B.K. Adjustable Frequency–Duty–Cycle Hybrid Control Strategy for Full-Bridge Series Resonant Converters in Electric Vehicle Chargers. *IEEE Trans. Ind. Electron.* **2014**, *61*, 5354–5362.
93. Vu, H.N.; Choi, W. A Novel Dual Full-Bridge LLC Resonant Converter for CC and CV Charges of Batteries for Electric Vehicles. *IEEE Trans. Ind. Electron.* **2018**, *65*, 2212–2225. [[CrossRef](#)]
94. Wei, Y.Q.; Luo, Q.M.; Du, X.; Altin, N.; Nasiri, A.; Alonso, J.M. A Dual Half-Bridge LLC Resonant Converter with Magnetic Control for Battery Charger Application. *IEEE Trans. Power Electron.* **2020**, *35*, 2196–2207. [[CrossRef](#)]
95. Musavi, F.; Craciun, M.; Gautam, D.S.; Eberle, W.G.; Dunford, W. An LLC Resonant DC-DC Converter for Wide Output Voltage Range Battery Charging Applications. *IEEE Trans. Power Electron.* **2013**, *28*, 5437–5445. [[CrossRef](#)]
96. Shen, Y.X.; Zhao, W.H.; Chen, Z.; Cai, C.C. Full-bridge LLC Resonant Converter with Series-parallel Connected Transformers for Electric Vehicle On-board Charger. *IEEE Access* **2018**, *6*, 13490–13500. [[CrossRef](#)]
97. Wei, Y.Q.; Luo, Q.M.; Mantooth, A. Hybrid Control Strategy for LLC Converter with Reduced Switching Frequency Range and Circulating Current for Hold-Up Time Operation. *IEEE Trans. Power Electron.* **2021**, *36*, 8600–8606. [[CrossRef](#)]

98. Li, H.R.; Zhang, Z.L.; Wang, S.D.; Tang, J.C.; Ren, X.Y.; Chen, Q.H. A 300-kHz 6.6-kW SiC Bidirectional LLC Onboard Charger. *IEEE Trans. Ind. Electron.* **2020**, *67*, 1435–1445. [[CrossRef](#)]
99. Zhao, L.; Pei, Y.Q.; Wang, L.L.; Pei, L.; Cao, W.; Gan, Y.M. Design Methodology of Bidirectional Resonant CLLC Charger for Wide Voltage Range Based on Parameter Equivalent and Time Domain Model. *IEEE Trans. Power Electron.* **2022**, *37*, 12041–12064. [[CrossRef](#)]
100. Min, J.; Ordonez, M. Bidirectional Resonant CLLC Charger for Wide Battery Voltage Range: Asymmetric Parameters Methodology. *IEEE Trans. Power Electron.* **2021**, *36*, 6662–6673. [[CrossRef](#)]
101. Lee, B.K.; Kim, J.P.; Kim, S.G.; Lee, J.Y. An Isolated/Bidirectional PWM Resonant Converter for V2G(H) EV On-Board Charger. *IEEE Trans. Veh. Technol.* **2017**, *66*, 7741–7750. [[CrossRef](#)]
102. Yan, Y.; Bai, H.; Foote, A.; Wang, W.B. Securing Full-Power-Range Zero-Voltage Switching in Both Steady-State and Transient Operations for a Dual-Active-Bridge-Based Bidirectional Electric Vehicle Charger. *IEEE Trans. Power Electron.* **2020**, *35*, 7506–7519. [[CrossRef](#)]
103. Shao, S.; Chen, H.; Wu, X.K.; Zhang, J.M.; Sheng, K. Circulating Current and ZVS-on of a Dual Active Bridge DC-DC Converter: A Review. *IEEE Access* **2019**, *7*, 50561–50572. [[CrossRef](#)]
104. Xue, L.X.; Shen, Z.Y.; Boroyevich, D.; Mattavelli, P.; Diaz, D. Dual Active Bridge-Based Battery Charger for Plug-in Hybrid Electric Vehicle with Charging Current Containing Low Frequency Ripple. *IEEE Trans. Power Electron.* **2015**, *30*, 7299–7307. [[CrossRef](#)]
105. Vazquez, N.; Liserre, M. Peak Current Control and Feed-Forward Compensation of a DAB Converter. *IEEE Trans. Ind. Electron.* **2020**, *67*, 8381–8391. [[CrossRef](#)]
106. Assadi, S.A.; Matsumoto, H.; Moshirvaziri, M.; Nasr, M.; Zaman, M.S.; Trescases, O. Active Saturation Mitigation in High-Density Dual-Active-Bridge DC-DC Converter for On-Board EV Charger Applications. *IEEE Trans. Power Electron.* **2020**, *35*, 4376–4387. [[CrossRef](#)]
107. Tran, D.; Vu, N.; Choi, W. A Quasi-Resonant ZVZCS Phase-Shifted Full-Bridge Converter with an Active Clamp in the Secondary Side. *Energies* **2018**, *11*, 2868. [[CrossRef](#)]
108. Lim, C.Y.; Jeong, Y.; Moon, G.W. Phase-Shifted Full-Bridge DC-DC Converter with High Efficiency and High Power Density Using Center-Tapped Clamp Circuit for Battery Charging in Electric Vehicles. *IEEE Trans. Power Electron.* **2019**, *34*, 10945–10959. [[CrossRef](#)]
109. Shi, K.M.; Zhang, D.L.; Gu, Y. Interleaved Current-Driven Phase-Shift Full-Bridge Converter with Magnetic Integration and Voltage Doubler Rectifiers. *IEEE Trans. Power Electron.* **2018**, *33*, 8308–8321. [[CrossRef](#)]
110. Liu, G.H.; Wang, B.X.; Liu, F.; Wang, X.Y.; Guan, Y.S.; Wang, W.; Wang, Y.J.; Xu, D.G. An Improved Zero-Voltage and Zero-Current-Switching Phase-Shift Full-Bridge PWM Converter With Low Output Current Ripple. *IEEE Trans. Power Electron.* **2023**, *36*, 3419–3432. [[CrossRef](#)]
111. Yang, Y.Z.; Li, H.J.; Wu, C.; Xu, J.Z.; Bi, Y.X.; Zhao, Y. An Improved Control Scheme for Reducing Circulating Current and Reverse Power of Bidirectional Phase-Shifted Full-Bridge Converter. *IEEE Trans. Power Electron.* **2022**, *37*, 11620–11635. [[CrossRef](#)]
112. Escudero, M.; Meneses, D.; Rodriguez, N.; Morales, D.P. Modulation Scheme for the Bidirectional Operation of the Phase-Shift Full-Bridge Power Converter. *IEEE Trans. Power Electron.* **2020**, *35*, 1377–1391. [[CrossRef](#)]
113. Guo, Z.Q.; Zhu, Y.Q.; Sha, D.S. Zero-Voltage-Switching Asymmetrical PWM Full-Bridge DC-DC Converter with Reduced Circulating Current. *IEEE Trans. Ind. Electron.* **2021**, *68*, 3840–3853. [[CrossRef](#)]
114. Rasool, H.; Verbrugge, B.; Jaman, S.; Abramushkina, E.; Geury, T.; El Baghdadi, M.; Hegazy, O. Design and Real-Time Implementation of a Control System for SiC Off-Board Chargers of Battery Electric Buses. *Energies* **2022**, *15*, 1434. [[CrossRef](#)]
115. Parvez, M.; Mekhilef, S.; Tan, N.M.L.; Akagi, H. Model Predictive Control of a Bidirectional AC-DC Converter for V2G and G2V Applications in Electric Vehicle Battery Charger. In Proceedings of the 2014 IEEE Transportation Electrification Conference and Expo (ITEC), Dearborn, MI, USA, 15–18 June 2014.
116. Alfaro, C.; Guzman, R.; de Vicuña, L.G.; Miret, J.; Castilla, M. Dual-Loop Continuous Control Set Model Predictive Control for a Three-phase Unity Power Factor Rectifier. *IEEE Trans. Power Electron.* **2021**, *37*, 1447–1460.
117. Jiao, R.; Zhu, J.; Ma, L.F.; Zhao, Y.T.; Zhang, B.Q.; Ding, Y.F.; Gong, C.; Yang, S. Dead-beat Instantaneous Power Control for Off-board Charger of Electric Vehicle for V2G Application. *Int. J. Hydrogen Energy* **2017**, *42*, 18174–18180. [[CrossRef](#)]
118. Wei, R.; Liu, Z.J.; Zhou, K.; Xu, L.; Xu, B.W. Frequency Control in Distribution Feeders Based on Bidirectional V2G Converter for EV. In Proceedings of the 2017 IEEE Conference on Energy Internet and Energy System Integration (EI2), Beijing, China, 26–28 November 2017; pp. 1–5.
119. Song, W.Z.; Yu, F.; Dai, Z.H.; He, Z.X.; Yu, H.; Xing, F.X.; Yan, H. Proportional resonant current control strategy with load current feed-forward control for VIENNA rectifier. *Electr. Mach. Control* **2019**, *23*, 76–83.
120. Nair, H.S.; Lakshminarasamma, N. An Improved FS-MPC Algorithm for Vienna Rectifier Based EV Chargers. In Proceedings of the 2020 IEEE Transportation Electrification Conference & Expo (ITEC), Chicago, IL, USA, 23–26 June 2020; pp. 1103–1108.
121. Li, X.; Sun, Y.; Wang, H.; Su, M.; Huang, S.D. A Hybrid Control Scheme for Three-Phase Vienna Rectifiers. *IEEE Trans. Power Electron.* **2018**, *33*, 629–640. [[CrossRef](#)]
122. Xu, G.J.; Wang, C. Control Strategy for Neutral-point Voltage Balance of Three-phase VIENNA Rectifier Based on One-cycle Control. *J. Power Sup.* **2018**, *16*, 9–15.
123. Dang, C.L.; Tong, X.Q.; Song, W.Z. Discrete Sliding Mode Control Strategy for A Three-phase Boost-type VIENNA Rectifier with the CB-PWM. *IEEJ Trans. Electr. Electron. Eng.* **2020**, *15*, 607–615. [[CrossRef](#)]

124. Zhang, M.; Yuan, Y.; Sun, X.; Zhang, Y.; Li, X. Harmonic Resonance Suppression Strategy of the Front-End Vienna Rectifier in EV Charging Piles. *IEEE Trans. Power Electron.* **2023**, *38*, 1036–1053. [[CrossRef](#)]
125. Guo, Q.; Liu, H.P.; Peng, D.L.; Liu, Q.; Zhang, Y. A Multi-loop Control Strategy and Parameter Design for Current-source PWM Rectifiers. *Proc. Chin. Soc. Elect. Eng.* **2015**, *35*, 1193–1202.
126. Huang, R.; Xu, J.; Chen, Q.; Guo, X.; Cao, H. Reconstructed Phase Voltages Based Power Following Control for Three-Phase Buck Rectifier Under Unbalanced Phase Voltages and Wide AC Input Frequency. *IEEE Trans. Power Electron.* **2023**, *38*, 2022–2031. [[CrossRef](#)]
127. Chen, Q.; Xu, J.P.; Huang, R.; Wang, W.S.; Wang, L. A Digital Control Strategy with Simple Transfer Matrix for Three-Phase Buck Rectifier Under Unbalanced AC Input Conditions. *IEEE Trans. Power Electron.* **2021**, *36*, 3661–3666. [[CrossRef](#)]
128. Cortes, P.; Vancu, M.F.; Kolar, J.W. Swiss Rectifier Output Voltage Control with Inner Loop Power Flow Programming (PFP). In Proceedings of the 2013 IEEE 14th Workshop on Control and Modeling for Power Electronics (COMPEL), Salt Lake City, UT, USA, 23–26 June 2013; pp. 1–8.
129. Jia, Q.; Qi, Y.C.; Xiong, X.; Ma, P.W. Research and Implementation of SWISS Rectifier Based on Fuzzy PI Control. In Proceedings of the 2018 3rd International Conference on Mechanical, Control and Computer Engineering (ICMCCE), Huhhot, China, 14–16 September 2018; pp. 31–36.
130. Schrittwieser, L.; Kolar, J.W.; Soeiro, T.B. Novel SWISS Rectifier Modulation Scheme Preventing Input Current Distortions at Sector Boundaries. *IEEE Trans. Power Electron.* **2017**, *32*, 5771–5785. [[CrossRef](#)]
131. Chen, R.R.; Yao, Y.; Zhao, L.; Xu, M. Inhibiting Mains Current Distortion for SWISS Rectifier—A Three-phase Buck-type Harmonic Current Injection PFC Converter. In Proceedings of the 2015 IEEE Applied Power Electronics Conference and Exposition (APEC), Charlotte, NC, USA, 15–19 March 2015; pp. 1850–1854.
132. Sha, D.S.; Xu, G.; Xu, Y.X. Utility Direct Interfaced Charger/Discharger Employing Unified Voltage Balance Control for Cascaded H-Bridge Units and Decentralized Control for CF-DAB Modules. *IEEE Trans. Ind. Electron.* **2017**, *64*, 7831–7841. [[CrossRef](#)]
133. Abronzini, U.; Attaianesi, C.; D’Arpino, M.; Di Monaco, M.; Rufer, A.; Tomasso, G. Dead Time and Non-linearities Compensation for CHB Multi-level Converters with Integrated ESS Feeding EV’s Ultra-fast Charging Stations. In Proceedings of the 2016 International Conference on Electrical Systems for Aircraft, Railway, Ship Propulsion and Road Vehicles & International Transportation Electrification Conference (ESARS-ITEC), Toulouse, France, 2–4 November 2016; pp. 1–5.
134. Drobic, K.; Grandi, G.; Hammami, M.; Mandrioli, R.; Ricco, M.; Viatkin, A.; Vujacic, M. An Output Ripple-Free Fast Charger for Electric Vehicles Based on Grid-Tied Modular Three-Phase Interleaved Converters. *IEEE Trans. Ind. Appl.* **2019**, *55*, 6102–6114. [[CrossRef](#)]
135. Tesaki, K.; Hagiwara, M. Control and Experimental Verification of a Bidirectional Non-isolated DC-DC Converter Based on Switched-Capacitor Converters. *IEEE Trans. Power Electron.* **2021**, *36*, 6501–6512. [[CrossRef](#)]
136. Razani, R.; Mohamed, Y.A.R.I. Model Predictive Control of Non-Isolated DC/DC Modular Multilevel Converter Improving the Dynamic Response. *IEEE Open J. Power Electron.* **2022**, *3*, 303–316. [[CrossRef](#)]
137. Schuck, M.; Pilawa-Podgurski, R.C.N. Ripple Minimization Through Harmonic Elimination in Asymmetric Interleaved Multi-phase DC-DC Converters. *IEEE Trans. Power Electron.* **2015**, *30*, 7202–7214. [[CrossRef](#)]
138. Awasthi, A.; Bagawade, S.; Jain, P.K. Analysis of a Hybrid Variable Frequency-Duty Cycle Modulated low-Q LLC Resonant Converter for Improving Light-Load Efficiency for Wide Input Voltage Range. *IEEE Trans. Power Electron.* **2021**, *36*, 8476–8493. [[CrossRef](#)]
139. Feng, W.Y.; Lee, F.C.; Mattavelli, P. Simplified Optimal Trajectory Control (SOTC) for LLC Resonant Converters. *IEEE Trans. Power Electron.* **2013**, *28*, 457–466. [[CrossRef](#)]
140. Fei, C.; Li, Q.; Lee, F.C. Digital Implementation of Light-Load Efficiency Improvement for High-Frequency LLC Converters with Simplified Optimal Trajectory Control. *IEEE J. Emerg. Sel. Top. Power Electron.* **2018**, *6*, 1850–1859. [[CrossRef](#)]
141. Moon, S.C.; Chiu, C.H. Hybrid-Mode PFM Control for LLC Resonant Converter. *IEEE Trans. Power Electron.* **2022**, *37*, 274–284. [[CrossRef](#)]
142. Chen, J.B.; Yang, C.Y.; Tang, S.Z.; Zou, J.J. A High Power Interleaved Parallel Topology Full-Bridge LLC Converter for Off-Board Charger. *IEEE Access* **2021**, *9*, 157790–157799. [[CrossRef](#)]
143. Park, H.P.; Jung, J.H. PWM and PFM Hybrid Control Method for LLC Resonant Converters in High Switching Frequency Operation. *IEEE Trans. Ind. Electron.* **2017**, *64*, 253–263. [[CrossRef](#)]
144. Kim, J.H.; Kim, C.E.; Kim, J.K.; Lee, J.B.; Moon, G.W. Analysis on Load-Adaptive Phase-Shift Control for High Efficiency Full-Bridge LLC Resonant Converter Under Light-Load Conditions. *IEEE Trans. Power Electron.* **2016**, *31*, 4942–4955.
145. Wu, H.F.; Zhan, X.H.; Xing, Y. Interleaved LLC Resonant Converter with Hybrid Rectifier and Variable-Frequency Plus Phase-Shift (VFPPS) Control for Wide Output Voltage Range Applications. *IEEE Trans. Power Electron.* **2017**, *32*, 4246–4257. [[CrossRef](#)]
146. Hou, N.; Li, Y.W. Overview and Comparison of Modulation and Control Strategies for Non-Resonant Single-Phase Dual-Active-Bridge Dc-Dc Converter. *IEEE Trans. Power Electron.* **2020**, *35*, 3148–3172. [[CrossRef](#)]
147. Bai, H.; Nie, Z.L.; Mi, C.T. Experimental Comparison of Traditional Phase-Shift, Dual-Phase-Shift, and Model-Based Control of Isolated Bidirectional DC-DC Converters. *IEEE Trans. Power Electron.* **2010**, *25*, 1444–1449. [[CrossRef](#)]
148. Segaran, D.; Holmes, D.G.; McGrath, B.P. Enhanced Load Step Response for a Bidirectional DC-DC Converter. *IEEE Trans. Power Electron.* **2013**, *28*, 371–379. [[CrossRef](#)]

149. Oggier, G.G.; Ordonez, M.; Galvez, J.M.; Luchino, F. Fast Transient Boundary Control and Steady-State Operation of the Dual Active Bridge Converter Using the Natural Switching Surface. *IEEE Trans. Power Electron.* **2014**, *29*, 946–957. [[CrossRef](#)]
150. Song, W.S.; Hou, N.; Wu, M.Y. Virtual Direct Power Control Scheme of Dual Active Bridge DC-DC Converters for Fast Dynamic Response. *IEEE Trans. Power Electron.* **2018**, *33*, 1750–1759. [[CrossRef](#)]
151. Jeung, Y.C.; Lee, D.C. Voltage and Current Regulation of Bi-directional Isolated Dual Active Bridge DC-DC Converters based on Double-Integral Sliding Mode Control. *IEEE Trans. Power Electron.* **2019**, *34*, 6937–6946. [[CrossRef](#)]
152. Jin, S.; Chen, L.; Zhou, Z.H. Discrete Extended-Phase-Shift Control for Dual-Active-Bridge DC-DC Converter with Fast Dynamic Response. *IEEE Trans. Ind. Electron.* **2023**, *70*, 5662–5673.
153. Mishra, D.; Singh, B.; Panigrahi, B.K. Adaptive Current Control for a Bidirectional Interleaved EV Charger with Disturbance Rejection. *IEEE Trans. Ind. Appl.* **2021**, *57*, 4080–4090. [[CrossRef](#)]
154. Shih, L.C.; Liu, Y.H.; Chiu, H.J. A Novel Hybrid Mode Control for Phase-shift Full Bridge Converter Featuring High Efficiency over Full Load Range. *IEEE Trans. Power Electron.* **2019**, *34*, 2794–2804. [[CrossRef](#)]
155. Kanamarlapudi, V.R.K.; Wang, B.F.; Kandasamy, N.K.; So, P.L. A New ZVS Full-Bridge DC-DC Converter for Battery Charging with Reduced Losses Over Full-Load Range. *IEEE Trans. Ind. Appl.* **2018**, *54*, 571–579. [[CrossRef](#)]
156. Yao, Y.; Kulothungan, G.S.; Krishnamoorthy, H.S. Improved Circuit Design and Adaptive Burst Mode Control in PSFB Converters for Higher Efficiency Over a Wide Power Range. *IEEE Access* **2022**, *10*, 9152–9163. [[CrossRef](#)]
157. Bak, Y.; Lee, Y.J.; Lee, K.B. Dynamic Characteristic Improvement of Phase-Shift Full-Bridge Center-Tapped Converters Using a Model Predictive Control. *IEEE Trans. Ind. Electron.* **2022**, *69*, 1488–1497. [[CrossRef](#)]
158. Saeed, J.; Wang, L.P.; Fernando, N. Model Predictive Control of Phase Shift Full-Bridge DC-DC Converter Using Laguerre Functions. *IEEE Trans. Contr. Syst. Technol.* **2022**, *30*, 819–826. [[CrossRef](#)]
159. Darcovich, K.; Recoskie, S.; MacNeil, D.D.; Darcovich, A. Operational intra-cycle temporal and current mode effects on battery capacity loss. *eTransportation* **2022**, *13*, 100185. [[CrossRef](#)]
160. Zhang, Z.G.; Zhang, T.; Tang, A.H. A review of fast charging methods for vehicle lithium batteries under healthy conditions. *J. Southwest Univ. (Nat. Sci. Ed.)* **2022**, *44*, 194–206.
161. Du, Q.; Zhang, Y.M.; Tian, S. The formation mechanism and formation process of SEI film in lithium ion battery. *Power Supply Technol.* **2018**, *42*, 1922–1926.
162. Yang, X.; Wang, C.Y. Understanding the Trilemma of Fast Charging, Energy Density and Cycle Life of Lithium-Ion Batteries. *J. Power Sources* **2018**, *402*, 489–498. [[CrossRef](#)]
163. Zhou, X.; Zhou, P.; Zheng, Y.J.; Han, X.B.; Zhu, Z.Y.; Liu, J.H.; Yang, Y.H.; Xue, G. Lithium-ion battery wide temperature range lithium-free fast charging strategy. *J. Automot. Saf. Energy Sav.* **2020**, *11*, 397–405.
164. Zhang, B.H.; Chen, M.; Yang, D.M. Investigation of the polarization effect in lithium iron phosphate battery for electric vehicles. In Proceedings of the 2014 IEEE Conference and Expo Transportation Electrification Asia-Pacific (ITEC Asia-Pacific), Beijing, China, 31 August–3 September 2014; pp. 1–5.
165. Di, Y.M.; Jiae, Y.; Daejin, P.; Cho, J. Dynamic Frequency and Duty Cycle Control Method for Fast Pulse-Charging of Lithium Battery Based on Polarization Curve. In Proceedings of the 2015 Ninth International Conference on Frontier of Computer Science and Technology, Dalian, China, 26–28 August 2015; pp. 40–45.
166. Liu, L.; Wang, F.; Fan, B.; He, X.; Ren, S. The application of thermal characteristics method in the study of fast charging performance of power battery. *Power Supply Technol.* **2018**, *42*, 365–366+372.
167. Jaguemont, J.; Abdel-Monem, M.; Omar, N.; Mierlo, J.V.; Bossche, P.V.D. Thermal Effect of Fast-Charging Profiles on Lithium-Ion Batteries. In Proceedings of the 2018 21st International Conference on Electrical Machines and Systems (ICEMS), Jeju, South Korea, 7–10 October 2018; pp. 2127–2132.
168. Du, J.Y.; Sun, Y.Z. The Influence of High Power Charging on the Lithium Battery Based on Constant and Pulse Current Charging Strategies. In Proceedings of the 2020 IEEE Vehicle Power and Propulsion Conference (VPPC), Gijon, Spain, 18 February 2020; pp. 1–7.
169. Yin, P.X.; Wang, N.; Shang, Y.L.; Gu, P.W.; Duan, B.; Zhang, C.H. Study on the Effect of High Temperature and High-Current Rate on Fast Charging of Lithium-ion Batteries. In Proceedings of the 2021 40th Chinese Control Conference (CCC), Shanghai, China, 26–28 July 2021; pp. 5841–5846.
170. Duru, K.K.; Karra, C.; Venkatachalam, P.; Betha, S.A.; Madhavan, A.A.; Kalluri, S. Critical Insights into Fast Charging Techniques for Lithium-Ion Batteries in Electric Vehicles. *IEEE Trans. Device Mater. Reliab.* **2021**, *21*, 137–152. [[CrossRef](#)]
171. Chen, C.L.; Wei, Z.B.; Knoll, A.C. Charging Optimization for Li-Ion Battery in Electric Vehicles: A Review. *IEEE Trans. Transp. Electr.* **2022**, *8*, 3068–3089. [[CrossRef](#)]
172. Huang, X.R.; Liu, W.J.; Acharya, A.B.; Meng, J.H.; Teodorescu, R.; Stroe, D. Effect of Pulsed Current on Charging Performance of Lithium-Ion Batteries. *IEEE Trans. Ind. Electron.* **2022**, *69*, 10144–10153. [[CrossRef](#)]
173. Huang, X.R.; Liu, W.J.; Meng, J.H.; Li, Y.Y.; Jin, S.Y.; Teodorescu, R.; Stroe, D. Lifetime Extension of Lithium-ion Batteries with Low-Frequency Pulsed Current Charging. *IEEE J. Emerg. Sel. Top. Power Electron.* **2023**, *11*, 57–66. [[CrossRef](#)]
174. Wu, X.G.; Xia, Y.L.; Du, J.Y.; Gao, X.J.; Nikolay, S. Multi-Stage Constant Current Charging Strategy Based on Multi-Objective Current Optimization. *IEEE Trans. Transp. Electr.* **2022**; *Early Access*.

175. Ding, Z.Y.; Iam, I.W.; Ieong, C.F.; Lam, C.S. A Bivariate Control Strategy on Inductive Power Transfer Converter for Multi-Stage Constant Current Charging. In Proceedings of the IECON 2022 48th Annual Conference of the IEEE Industrial Electronics Society (ACIIES), Brussels, Belgium, 17–20 October 2022; pp. 1–5.
176. Wu, T.Z.; Lu, C.D.; Huang, Z.Y. A method to improve the energy utilization rate of lithium battery pulse charging. *Power Supply Technol.* **2020**, *44*, 1775–1778+1799.
177. Ye, M.; Gong, H.R.; Xiong, R.; Mu, H. Research on the Battery Charging Strategy with Charging and Temperature Rising Control Awareness. *IEEE Access* **2018**, *6*, 64193–64201. [[CrossRef](#)]
178. Jeon, S.U.; Park, J.W.; Kang, B.K.; Lee, H.J. Study on Battery Charging Strategy of Electric Vehicles Considering Battery Capacity. *IEEE Access* **2021**, *9*, 89757–89767. [[CrossRef](#)]
179. Nuamkoksung, P.; Buayai, K.; Kongjeen, Y.; Bhumkittipich, K.; Kerdchen, K.; Mithulanathan, N. Impact of Fast Charging on Lithium-ion Battery in Electric Vehicle Application. In Proceedings of the 2020 8th International Electrical Engineering Congress (IEECON), Chiang Mai, Thailand, 4–6 March 2020; pp. 1–4.
180. Mishra, S.; Swain, S.C.; Samantaray, R.K. A Review on Battery Management system and its Application in Electric vehicle. In Proceedings of the 2021 International Conference on Advances in Computing and Communications (ICACC), Kakknad, India, 21–23 October 2021; pp. 1–6.
181. Piao, N.; Gao, X.N.; Yang, H.C.; Guo, Z.Q.; Hu, G.J.; Cheng, H.M.; Li, F. Challenges and development of lithium-ion batteries for low temperature environments. *eTransportation* **2022**, *11*, 100145. [[CrossRef](#)]
182. Kumar, P.; Rankin, G.; Pattipati, K.R.; Balasingam, B. Model-Based Approach to Long Term Prediction of Battery Surface Temperature. *IEEE J. Emerg. Sel. Top. Ind. Electron.* **2023**, *4*, 389–399. [[CrossRef](#)]
183. Peng, X.B.; Garg, A.; Zhang, J.; Shui, L. Thermal management system design for batteries packs of electric vehicles: A survey. In Proceedings of the 2017 Asian Conference on Energy, Power and Transportation Electrification (ACEPT), Singapore, 24–26 October 2017; pp. 1–5.
184. Liu, Y.; Zhang, C.P.; Jiang, J.C.; Zhang, L.J.; Zhang, W.G.; Wang, L.Y. Deduction of the transformation regulation on voltage curve for lithium-ion batteries and its application in parameters estimation. *eTransportation* **2022**, *12*, 100164. [[CrossRef](#)]
185. Zhao, L.H.; Qin, P.L. Accurate SOC Prediction and Monitoring of Each Cell in a Battery Pack Considering Various Influencing Factors. *IEEE Tran. Ind. Electr.* **2023**, *70*, 1025–1035. [[CrossRef](#)]
186. Xiong, R.; Zhang, Y.Z.; Wang, J.; He, H.W.; Peng, S.M.; Pecht, M. Lithium-Ion Battery Health Prognosis Based on a Real Battery Management System Used in Electric Vehicles. *IEEE Tran. Veh. Technol.* **2019**, *68*, 4110–4121. [[CrossRef](#)]
187. Hecht, C.; Victor, K.; Zurmühlen, S.; Sauer, D.U. Electric vehicle route planning using real-world charging infrastructure in Germany. *eTransportation* **2021**, *10*, 100143. [[CrossRef](#)]
188. Jia, L.; Hu, Z.C.; Liang, W.J.; Lang, W.Z.; Song, Y.H. A novel approach for urban electric vehicle charging facility planning considering combination of slow and fast charging. In Proceedings of the 2014 International Conference on Power System Technology, Chengdu, China, 20–22 October 2014; pp. 3354–3360.
189. Franzese, P.; Patel, D.D.; Mohamed, A.A.; Lannuzzi, D.; Fahimi, B.; Risso, M.; Miller, J.M. Fast DC Charging Infrastructures for Electric Vehicles: Overview of Technologies, Standards, and Challenges. *IEEE Trans. Transp. Electrif.* **2023**, *1*, 121–134. [[CrossRef](#)]
190. Parchomiuk, M.; Moradewicz, A.; Gawiński, H. An Overview of Electric Vehicles Fast Charging Infrastructure. In Proceedings of the 2019 Progress in Applied Electrical Engineering (PAEE), Koscielisko, Poland, 17–21 June 2019; pp. 1–5.
191. Matanov, N.; Zahov, A. Developments and Challenges for Electric Vehicle Charging Infrastructure. In Proceedings of the 2020 12th Electrical Engineering Faculty Conference (Bulef), Varna, Bulgaria, 9–12 September 2020; pp. 1–5.
192. Trinko, D.; Horesh, N.; Zane, R.; Song, Z.Q.; Kaminen, A.; Konstantinou, T.; Gkritza, K.; Quinn, C.; Bradley, T.H.; Quinn, J.C. Economic feasibility of in-motion wireless power transfer in a high-density traffic corridor. *eTransportation* **2022**, *11*, 100154. [[CrossRef](#)]
193. Yuan, N.N.; Yu, Z.Z.; Zhang, Y.F.; Chang, H.J.; Kang, H.W. Review of Electric Vehicle Ultra-Fast DC Charging Station. In Proceedings of the 2022 7th Asia Conference on Power and Electrical Engineering (ACPEE), Hangzhou, China, 15–17 April 2022; pp. 1–9.
194. IT Home. Audi Launches A6 Avant e-Tron Pure Tram: 700 km Endurance. 2024. Available online: <https://www.ithome.com/0/608/135.htm> (accessed on 17 March 2022).
195. Che, Y. Volkswagen SSP Pure Electric Platform Is Looking Forward to 2025 Production/Coverage of Audi Porsche and other Brands. Available online: <https://baijiahao.baidu.com/s?id=1732275172168757738> (accessed on 9 May 2022).
196. Tencent. This Paper Analyzes the Battery and Charging Scheme of Modern E-GMP Electric Vehicle Platform. Available online: <https://new.qq.com/rain/a/20201207A04AJ800> (accessed on 7 December 2020).
197. Tencent. It Is Reported That NIO will Lay Out Million-Yuan Electric Vehicles. Available online: <https://new.qq.com/rain/a/20230110A090GH00> (accessed on 10 January 2023).
198. Sina Technology. Ideal Automobile Product Planning: Research and Development of High-Voltage Pure Electric Platform, Launch Two Pure Electric SUVs in 2023. Available online: <https://finance.sina.com.cn/tech/2021-07-26/doc-ikqcfncna9059959.shtml> (accessed on 26 July 2021).
199. Sina Automobile. In the Future, There Will Be Three New Models BYD e Platform 3.0 Analysis. Available online: <https://auto.sina.com.cn/jishu/2021-09-09/detail-iktzqtyt4867281.shtml> (accessed on 9 September 2021).

200. Tencent. Chang'an Automobile Issued a New Generation of Super Collector Drive, C385 for the First Time with a Stunning Appearance. Available online: <https://new.qq.com/rain/a/20210825A0307R00> (accessed on 25 August 2021).
201. Shu, Q.; Wang, Y.F.; Liang, Y. Status and Prospect of Safety Standards for Electric Vehicle Power Battery in China. *Automot. Eng.* **2022**, *44*, 1706–1715.
202. Dixon, J.; Bukhsh, W.; Bell, K.; Brand, C. Vehicle to grid: Driver plug-in patterns, their impact on the cost and carbon of charging, and implications for system flexibility. *eTransportation* **2022**, *13*, 100180. [[CrossRef](#)]
203. Darcovich, K.; Recoskie, S.; Ribberink, H.; Michelet, C. The impact of V2X service under local climatic conditions within Canada on EV durability. *eTransportation* **2021**, *9*, 100124. [[CrossRef](#)]
204. Liu, S.G.; Ye, Z.X. Progress and Prospect of Electric Vehicle's V2G Technology. In Proceedings of the 2019 6th International Conference on Information Science and Control Engineering (ICISCE), Shanghai, China, 20–22 December 2019; pp. 412–416.

Disclaimer/Publisher's Note: The statements, opinions and data contained in all publications are solely those of the individual author(s) and contributor(s) and not of MDPI and/or the editor(s). MDPI and/or the editor(s) disclaim responsibility for any injury to people or property resulting from any ideas, methods, instructions or products referred to in the content.